Title:

Segment-specific axon guidance by Wnt/Fz signaling diversifies motor commands in *Drosophila* larvae

Authors:

Suguru Takagi [1, #], Shiina Takano [1], Yusaku Hashimoto [1], Shu Morise [1], Xiangsunze Zeng [1], and Akinao Nose [1,2,3,*]

Affiliations:

[1] Department of Complexity Science and Engineering, Graduate School of Frontier Sciences, The University of Tokyo, Chiba, 277-8561, Japan

[2] Department of Physics, Graduate School of Science, The University of Tokyo, Tokyo, 113-0033, Japan

[3] Lead contact

[*] Corresponding author

[#] Present address: Center for Integrative Genomics, Faculty of Biology and Medicine, University of Lausanne, 1015 Lausanne, Switzerland

Summary

What developmental mechanisms underlie functional diversification of neural circuits? We address this question in *Drosophila* larvae by focusing on segmentally homologous Wave command neurons, which diversify their wiring and function in a location-specific manner. Anterior Wave (a-Wave) neurons extend axons anteriorly and connect to circuits inducing backward locomotion, whereas posterior Wave (p-Wave) neurons extend axons posteriorly and trigger forward locomotion. Here, we show that Frizzled receptors DFz2 and DFz4, together with the DWnt4 ligand, regulate the segment-specific Wave axon projection. *DFz2* knock-down (KD) not only reroutes a-Wave axons to posterior neuromeres but also biases its motor command to induce forward instead of backward locomotion. Thus, segment-specific axon guidance diversifies the function of homologous command neurons in behavioral regulation. Since control of anterior-posterior (A-P) axon guidance by Wnt/Fz-signaling is evolutionarily conserved, our results reveal a potentially universal principle for formation and diversification of the command system in the nerve cord.

Keywords

Drosophila, axon guidance, segment specificity, action selection, tactile circuit, sensory-motor transformation, Frizzled, Wnt, optogenetics, RNAi

Introduction

The adaptive behavior of an animal is underpinned by the complex yet precise connectivity of its nervous system. For ecologically fit behaviors to occur, information regarding various sensory inputs must be routed to appropriate motor outputs during development. Although much work has revealed the molecular and cellular bases of neurite guidance and synapse formation (Kolodkin and Tessier-Lavigne, 2011; Tessier-Lavigne and Goodman, 1996; Tosches, 2017), the relationship between principles of neural wiring and behavioral regulation remains obscure.

The evolution of the nervous system commonly involves the diversification of homologous circuits (Chakraborty and Jarvis, 2015; Tosches, 2017), which is observed in a wide range of brain regions including spinal segments (Leung and Shimeld, 2019; Levine et al., 2012), basal ganglia (Grillner and Robertson, 2016), cerebral (Tosches et al., 2018), and cerebellar (Kebschul et al., 2021) cortices. For instance, the spinal cord in vertebrates and ventral nerve cord (VNC) in invertebrates are composed of homologous neuromeres, which link inputs from the corresponding body segment to appropriate motor output(s) (Barthélemy et al., 2006; Levine et al., 2014; Saltiel et al., 1998; Takagi et al., 2017; Tresch and Bizzi, 1999). Accordingly, adaptive behaviors may be established in part by diversifying the connectivity within homologous circuits, through changes in the circuit's wiring during development. However, whether such a mechanism does play a role in diversifying behaviors remains unclear (Chakraborty and Jarvis, 2015; Katz, 2011; Kirschner and Gerhart, 1998; Tosches, 2017). Since the circuit wiring process not only includes stepwise interactions with various surrounding cells during development but also matching among a number of pre- and postsynaptic cells, circuit diversification may require orchestrated changes in the expression of a large number of genes. Alternatively, there may be some degree of flexibility in the system such that modulation of a

small number of architectural features/properties (e.g. changes in the expression of neurite guidance molecules in a small population of cells) is sufficient to alter an animal's behavior. It has been generally difficult to address these questions due to the lack of tools to visualize and manipulate neural wiring in homologous circuits and our limited knowledge on the relationship between neurite guidance and behavioral regulation.

Previously, we identified a class of segmentally homologous command-like neurons in the VNC of *Drosophila* larvae, named Wave neurons (Takagi et al., 2017), which adaptively link tactile inputs from different segments to appropriate motor outputs (Figure 1A and A') by diversifying their connectivity. Wave neurons are present in identical positions in each abdominal neuromere, A1-A7, and extend their proximal axons to the neuropile in similar manners (Figure 1A-C). However, there is a striking difference in their longitudinal axon projection upon entering the neuropile and subsequent formation of functional connectivity. Wave neurons in anterior segments (a-Wave; in neuromeres A1-A3) extend axons anteriorly and connect to circuits inducing backward locomotion, whereas Wave neurons in posterior segments (p-Wave; in neuromeres A4-A7) extend axons posteriorly and elicit forward locomotion.

Here, we studied the molecular mechanism(s) underlying the diverged Wave A-P axon projections. We focused on Wnt receptors (Frizzled/Ryk) as they were known to be involved in bidirectional A-P axon guidance in mammals and nematodes (Hilliard and Bargmann, 2006; Kirszenblat et al., 2011; Lyuksyutova et al., 2003; Salinas and Zou, 2008). We found that Wave A-P axon projections are regulated by *Drosophila* Frizzled-2 (DFz2) and Frizzled-4 (DFz4) receptors, together with the Wnt4 (DWnt4) ligand. Intriguingly, *DFz2* KD not only rerouted a-Wave axons towards posterior neuromeres but also made a-Wave neurons induce fast-forward instead of backward locomotion, as p-Wave neurons do, suggesting that segment-specific axon

guidance determines the divergent roles of homologous command neurons in behavioral regulation. Our finding that changes in a single gene (*DFz2*) in one class of neuron (Wave) suffices to change the motor outputs of the animals, suggests that these circuits can be flexibly tuned to encode divergent behaviors during development and evolution (i.e., evolvable; Kirschner and Gerhart, 1998; Katz, 2011).

Results

DFz2 and DFz4 regulate segment-specific Wave axon projection

We performed an RNAi-based KD of *Drosophila* Wnt receptors (*DFz, DFz2, DFz3, DFz4, drl, Drl-2, smo, Corin*) in Wave neurons (see Method details) and observed their neurite morphology using a GAL4 line that consistently targets Wave neurons from embryonic to larval stages (Figure S1). We identified two genes, *DFz2* and *DFz4*, as being possibly involved in the axon extension towards the posterior end. KD of *DFz2* elongated the axon extension towards the posterior end, whereas KD of *DFz4* shortened it (Figure S2A-D, $p = 2.38\times10^{-6}$, Chi-square test).

To further study the role of these receptors, we examined the morphology of single Wave neurons in *DFz2* KD animals using the MultiColor FlpOut (MCFO, Nern et al., 2015) technique. Axon extension towards the posterior end (but not towards the anterior end) was elongated both in a-Wave and p-Wave neurons by KD of *DFz2* by two independent RNAi constructs (A2-Wave to A6-Wave; Figures 1B-M, S2F and F'). Notably, the abnormal extension of Wave axons towards the posterior end is accompanied by presynaptic varicosities *en route* (Figure 1D and E), suggesting that ectopic synapses are formed in this region. The ectopic axon extension from a-Wave neurons intruded the region where p-Wave axons normally project to (Figure 1F-J), raising the possibility that a-Wave neurons gain connections to the circuits inducing forward locomotion as p-Wave neurons do. Conversely, overexpression of *DFz2* in Wave neurons resulted in the shortening of a-Wave (but not p-Wave) axon extension towards the posterior end (Figure 1K and L). In summary, DFz2 is necessary for the suppression of Wave neurite outgrowth towards the posterior end (Figure 1M), and such suppression might be important to diversify Wave neuron connectivity across segments. We also found a posterior

extension of the dendrites of Wave neurons in *DFz2* KD animals. However, the ectopic extension of dendrites was much shorter and occurred less frequently as compared to that of the axon, so that *DFz2* KD may not greatly affect the tactile receptive fields of Wave neurons (Figure S3). In particular, the conserved dendritic extension pattern suggests that a-Wave neurons still receive inputs from tactile sensory neurons in anterior segments in *DFz2* KD animals as in the wild type (Takagi et al., 2017). Thus, while it cannot be excluded that there are some changes in the inputs, the outputs are more likely to be rerouted by *DFz2* KD in a-Wave neurons.

We also examined single cell morphologies of Wave neurons in *DFz4* KD animals (Figure 2) and found that posterior axon extension of the most posterior p-Wave neuron (A6-Wave) is shortened (Figures 2A-I). This observation suggests that *DFz4* mediates attraction of the p-Wave axons towards the posterior end. Neither posterior extension of other Wave axons (Figure 2C-F) nor the anterior extension of A6 or other Wave axons (Figure 2C-G) was affected, implying that DFz4 promotes axon extension of Wave axons selectively in A6-Wave and towards the posterior (summarized in Figure 2J). Also, no abnormality was seen in the dendrites of a- or p-Wave neurons (data not shown). *DFz4* overexpression did not yield any obvious phenotype (Figure 2H and I), suggesting that DFz4 expression alone is not sufficient to change the axon extension of Wave neurons.

<u>DWnt4 is a graded cue that regulates A-P Wave axon guidance</u>

We next sought to identify the ligand(s) of DFz2/DFz4 receptors. We first examined the overall extension pattern of Wave neurites in four *Drosophila Wnt* mutants (*DWnt4*$^{C1/EMS23}$,

DWnt5^{400}, *DWnt6*^{KO}, and *DWnt8*^{KO1}) and found that p-Wave axon extension towards the posterior end was shortened in *DWnt4* mutants, similarly to *DFz4* KD animals (Figures S2E and 3A-C). DWnt4 is known to have binding affinity to both DFz2 and DFz4 (Wu and Nusse, 2002), making it a strong candidate as a shared ligand of these receptors. Further analyses using single-Wave labelling (using heat-shock FlpOut) also revealed abnormalities in a-Wave: posterior extension of a-Wave axons was elongated, as was observed in *DFz2* KD mutants (Figure 3D, E, and G). Additionally, a-Wave axon extension towards the anterior end was shortened in *DWnt4* mutants (Figures 3D, E, and F), which was not observed in DFz2 or DFz4 receptor KD animals, suggesting that DWnt4 regulates anterior extension of a-Wave via other receptor(s). The fact that *DWnt4* mutants recapitulated both of the phenotypes observed in *DFz2* and *DFz4* KD animals (Figure 3H) suggests that both DFz2 and DFz4 use DWnt4 as a cue to regulate the extension of Wave axons along the A-P axis but with opposite valences.

Polarized extension of axons along the A-P axis could be regulated by gradients of the guidance cues and/or their receptors (Kirszenblat et al., 2011; Lyuksyutova et al., 2003). We therefore asked if there is any difference in the expression of DWnt4 and DFz2 along the A-P axis in the VNC. It has been previously suggested that *DWnt4* mRNAs are strongly expressed at the posterior end of the VNC (Hessinger et al., 2017). Our analyses of *DWnt4* knock-in GAL4 line (*Wnt4*$^{MI03717\text{-}Trojan}$*-GAL4*) further confirmed that the expression of *DWnt4* shows a gradient with higher expression towards the posterior end of the VNC (Figure 4A and B). Furthermore, DWnt4 immunostaining revealed a similar gradient within the neuropil (Figures 4C and D, S4A and B), indicating that protein expression is also polarized. These observations support the notion that DWnt4 regulates axon guidance along the A-P axis by forming a gradient along the axis.

Next, we performed DFz2 immunostaining to investigate the receptor expression along the A-P axis. We observed a weak gradient of DFz2 expression along the A-P axis in the opposite direction to DWnt4, with a slightly higher level of expression in the anterior part of the VNC neuropil (Figures 4E and F, S4C and D). Collectively, these results are consistent with the idea that complementary expression of DWnt4 and DFz2 regulates Wave axon extension via repulsion: Wave axons with higher levels of DFz2 and thus with higher sensitivity to repulsive DWnt4 signaling extend to the anterior VNC where levels of DWnt4 are low (Figure 4G). Due to the lack of reagents that allow visualization of DFz4 expression, whether DFz4 also shows graded expression along the A-P axis remains to be determined. However, based on the phenotype of *DFz4* KD (Figure 2) and the expression of DWnt4, it is likely that DFz4 guides p-Wave axons posteriorly by recognizing DWnt4 as an attractive cue (Figure 4G).

Motor commands of a-Wave neurons are altered by *DFz2* KD

We next asked whether motor outputs are altered by *DFz2* KD in a-Wave neurons. Activation of a-Wave normally induces backward locomotion, whereas p-Wave triggers forward locomotion (Takagi et al., 2017). Axon projection of a-Wave is altered in *DFz2* KD animals so that the axons extend towards the posterior VNC region where p-Wave axons target. Does the change in axon guidance also alter the motor commands of a-Wave neurons, such that the neurons now gain command of forward locomotion as p-Wave neurons normally do?

To address this, we performed area-confined optogenetics in Wave neurons using an *ex vivo* preparation of the central nervous system in the third instar larvae as previously performed (Takagi et al., 2017) but with the new GAL4 driver *R60G09-GAL4* that allows RNAi in Wave

neurons during the embryonic stage and optogenetic manipulation in the larvae (Figure 5A). In brief, we monitored the fictive motor outputs (fictive forward/backward locomotion) by calcium imaging of motor neurons while optogenetically activating a-Waves and p-Waves. In the control group, anterior stimulation of Wave neurons (A1) triggered backward waves while posterior stimulation (A5) triggered forward waves (Figure 5B, D, and G), as previously reported (Takagi et al., 2017). Intriguingly, stimulation of *DFz2* KD a-Wave neurons triggered slightly fewer backward waves but more forward waves (Figure 5C, D, and E) compared to the control group, implying a functional change of a-Wave neurons. By contrast, stimulation of *DFz2* KD p-Wave triggered similar amounts of backward/forward waves as in the control group (Figure 5F and G), suggesting that p-Wave retains its original function. These data suggest that the motor command of a-Wave is biased towards forward locomotion by KD of *DFz2*.

To further examine the change in Wave neuron outputs by the manipulation of *DFz2*, we performed optogenetic stimulation of all Wave neurons *in vivo*, which is known to induce a mixture of fast-forward locomotion (that occurs in the context of escape from nociceptive inputs (Ohyama et al., 2013, 2015) and is considered a distinct behavior from normal forward locomotion of the larvae), backward locomotion, and roll/bend (Figure S5A). In control animals, as observed in the previous report (Takagi et al., 2017), the stimulation induced fast-forward locomotion (Figure S5B), backward locomotion (Figure S5B') and rolling (Figure S5B''). By contrast, in Wave>*DFz2-RNAi* animals, the stimulation induced fast-forward locomotion (Figure S5C) and rolling (Figure S5C'') but not backward locomotion (Figure S5C'). We found that the speed of the evoked fast-forward locomotion (during stimulation) was faster in *DFz2* knocked-down animals while the baseline speed was unchanged (Figures S5D and E), indicating that fast-forward locomotion is enhanced in *DFz2* KD animals. In summary, *DFz2*

KD in Wave neurons augments their motor command of fast-forward locomotion while diminishing that of backward locomotion. Taken together with the *ex vivo* experiment (Figure 5), our results suggest that *DFz2* KD reroutes a-Wave axons to the circuits inducing fast-forward instead of backward locomotion and thus alters their motor commands.

Altered behavioral response to tactile stimuli in *DFz2* KD larvae

The differential motor behaviors commanded by Wave neurons are triggered by tactile stimuli at different body parts (Figure 1A and A'; Takagi et al., 2017). Does the altered axon projection of Wave neurons in *DFz2* KD animals impact the behavioral response evoked by tactile stimuli? Specifically, does selective a-Wave activation by natural tactile stimuli in the head induce fast-forward instead of backward locomotion seen in the wild-type larvae (Figures 5 and S5)? We tested these possibilities by presenting freely behaving larvae with a gentle touch on their head using a von Frey filament, which activates a- but not p-Wave neurons (Takagi et al., 2017). The gentle touch responses are known to be stereotypic but range from weak to strong, continuation of forward crawls (score 0), halting followed by crawl resumption (score 1), turning followed by crawl resumption (score 2), backing-up once (score 3), and backing-up multiple times (score 4) in *D. melanogaster* larvae (Kernan et al., 1994, Figure 6A). We found that *DFz*2 KD with two different RNAi lines in Wave neurons reduced backward locomotion responses (scores 3 and 4) while increasing turning responses (score 2) to head touch (Figure 6B, B', C, and C'). Since turning is not induced by Wave activation (Takagi et al., 2017), it is likely that the increased turning is due to the disinhibition of turning-inducing pathways (through other second-order tactile interneurons) by the deterioration of the

backward-inducing pathway (through Wave). Additionally, the speed of forward locomotion after each touch (usually after turning) was faster in *DF*z2 knocked-down animals (Figure 6B'' and C''), implying that fast-forward locomotion was induced in response to tactile stimulus. Taken together, our results suggest that changes in the axon guidance of Wave neurons alters the behavioral strategy of the larvae in response to external stimuli by altering the neurons' command function from backward-inducing to fast-forward-inducing.

Discussion

To understand the circuit mechanisms underlying behavior, perturbation of neurons and circuits while observing the behavior has been a successful paradigm (Luo et al., 2018). Most studies linking change in nervous system perturbation and behavioral alteration are either changes in physiology and/or mainly in the sensory periphery (Ardesch et al., 2019; Kim et al., 2017; Seeholzer et al., 2018; Tinbergen, 1951). Here we revealed a link between axon guidance and circuit function by identifying molecular mechanisms underlying the divergent axon extension of segmentally homologous Wave neurons and showing changes in the axon guidance alter motor commands (Figure 6D). The results illustrate several crucial features on how neural circuits mediating adaptive sensorimotor transformation form during development, and on how the evolution of the nervous system might lead to the acquisition of new behaviors.

Universal roles of Wnt/Fz signaling in A-P neurite guidance

Secreted proteins Wnts and their receptors Frizzled are evolutionarily conserved families of proteins. Wnt/Fz signaling is known to regulate A-P axon pathfinding in the nervous system of mammals and *C. elegans* (Hilliard and Bargmann, 2006; Lyuksyutova et al., 2003; Salinas and Zou, 2008). For instance, commissural neurons in the mouse spinal cord after crossing the midline extend their axons anteriorly by recognizing an anterior-high gradient of Wnt4 via the Frizzled3 receptor (Lyuksyutova et al., 2003). Similarly, lin-44/Wnt and lin-17/Frizzled regulate the A-P extension of the PLM mechanosensory neuron in *C. elegans* (Hilliard and Bargmann, 2006). Although Wnt/Fz proteins are known to regulate axon guidance in *Drosophila* (e.g., Inaki et al., 2007; Sato et al., 2006; Yoshikawa et al., 2003), whether they play

roles in A-P neurite guidance in the nerve cord was not previously known. The present study demonstrates this in *Drosophila* and thus points to the universal roles played by Wnt/Fz signaling in A-P neurite guidance in the animal kingdom.

We have shown that Frizzled receptors DFz2 and DFz4 regulate A-P axon guidance of homologous Wave neurons in segment-specific manner and in opposite valences, presumably by using DWnt4 as a common external guidance cue. Our results suggest that DFz4 mediates attraction of posterior Wave neurons towards the source of DWnt4 at the posterior end, whereas DFz2 mediates repulsion of both anterior and posterior Wave neurons away from the DWnt4 source. Presence of two graded signaling systems with antagonistic effects may aid in establishing reliable A-P axon guidance as proposed by theoretical models (Gierer, 1987). Our functional analyses of DFz2 and DFz4 receptors support the idea that the two signaling systems cooperate to guide the projection of Wave axons along the A-P axis. While this study focused on Wave neurons, it is likely that Wnt/Fz signaling also regulates A-P guidance of many other longitudinal, since DFz2 immunoreactivity was seen on a large fraction of axons in the anterior VNC.

Diversification of segment-specific motor commands by Fz-signaling

The command neuron concept is a widely appreciated notion that a specific type of interneuron serves as a linking node between external inputs and appropriate motor outputs (Bouvier et al., 2015; Kupfermann and Weiss, 1978; Wiersma and Ikeda, 1964). For command neurons to function in adaptive manners, they must be precisely wired to appropriate upstream and downstream circuits (Faumont et al., 2012). Indeed, modulation of input connectivity to

command neurons is known to alter sensory-evoked behaviors (Tenedini et al., 2019; Valdes-Aleman et al., 2021). However, whether changes in command neuron axon guidance alter their motor outputs was unknown. More importantly, how homologous command neurons might diverge their function to encode adaptive behavior(s) has been a long-standing question.

Here, we showed that *DFz2* KD not only alters the axon projection of a-Wave neurons but also biases their motor commands from backward to forward locomotion. When optogenetically activated, *DFz2* KD a-Wave neurons triggered much less backward locomotion, while they acquired the ability to induce fast forward locomotion (Figures 5 and S5). Furthermore, the way the larvae react to external tactile stimuli at the head is also biased from backing-up to turning-and-running (Figure 6), by the manipulation of DFz2. It is noteworthy that manipulation of DFz2 only in Wave neurons causes such drastic changes in larval behavior, since other known secondary neurons downstream of touch sensors and nociceptors (Eschbach and Zlatic, 2020; Hu et al., 2020) should remain intact in our molecular manipulation. This suggests that specificity of Wave-mediated motor commands is crucial for the larval behavior.

Segmental units in the spinal cords in vertebrates and VNC in invertebrates receive sensory inputs from corresponding body segment(s) and reroute the information to distinct motor outputs. The fact that *DFz2* KD a-Wave neurons function like p-Wave neurons and induce forward locomotion suggests that posterior axon projection and connection with forward-inducing circuits are a default state of Wave neurons and that suppression of posterior extension by Wnt/DFz2 is required for a-Wave to connect to alternative downstream circuits (those inducing backward locomotion) and acquire an alternative motor command. Our results uncover a mechanism of how command function of segmentally homologous neurons can be diverged during development to realize various sensory-motor transformations.

Flexible modulation of motor commands by A-P axon guidance

Since the way in which the nervous system carries out sensory-to-motor transformation is different between animal species in order to meet their respective ecological niches, the connectivity must be able to change flexibly during the evolution of the nervous system. If and how such connectivity changes occur during evolution remains poorly understood (Katz, 2011, 2016; Tosches, 2017). While a few studies demonstrated that the evolution of nervous system functions is indeed accompanied by connectivity changes (Ardesch et al., 2019; Sakurai et al., 2011; Seeholzer et al., 2018), the underlying developmental mechanisms remain unknown. Since command neurons link specific sensory inputs to appropriate motor outputs, changes in their wiring are likely to be a powerful mechanism by which animals acquire new sensory-evoked behavioral strategies that match changing environments without perturbing the overall network stability. Here, we demonstrated a simple developmental mechanism that potentially mediates such evolutional process by showing that just rerouting the axon of a single command neuron (a-Wave) to an ectopic location (posterior neuromeres) is sufficient to change the behavior of the larvae. Our results suggest for the presence of robust neural mechanisms that enable the “plug-and-play” modulation of motor commands as follows.

First, simply guiding the axon to a novel position appears to be sufficient for synapse formation with alternative downstream circuits. Since a-Wave neurons acquired the ability to induce fast forward locomotion in *DFz2* KD animals, these neurons likely formed synapses with neural circuits that trigger the behavior, presumably the downstream targets of p-Wave. It is known that neurons have robust capacity to form synapses with non-target cells, for instance

when placed in an ectopic position or when normal targets are deleted (Bekkers and Stevens, 1991; Cash et al., 1992; Hassan and Hiesinger, 2015; Shen and Bargmann, 2003; Xu et al., 2019). Furthermore, since a-Wave and p-Wave neurons are segmental homologues and likely share a large fraction of gene expression including those involved in synapse formation, a-Wave neurons once placed in the target region of p-Wave may readily form synapses with the p-Wave targets.

Second, there appears to be mechanism(s) that suppress functional connectivity to alternative downstream circuits so that only one behavioral output is induced. While a-Wave neurons in *DFz2* KD animals form ectopic axon extension posteriorly, the original anterior axon extension, which normally connect to backward-inducing circuits, remains intact morphologically. Nonetheless, the ability of a-Wave to induce backward locomotion is greatly reduced and instead forward-inducing ability is conferred. This suggest that connectivity from a-Wave axons to backward-inducing circuits is functionally suppressed, possibly by weakening of functional synapses between the synaptic partners and/or via reciprocal inhibition between the antagonistic downstream circuits.

The finding that switching in motor commands can occur upon manipulation of a single gene in single class of neurons argues that the Wave circuitry can be easily modified through evolution (Kirschner and Gerhart, 1998) to meet the tactile ecological niches of respective species. Consistent with this notion, we observed that larval response to head touch, where Wave neurons play major roles (as discussed above), varies among closely related species of *Drosophila* (S. Takagi and A.N., unpublished data). These results suggest that there is a certain degree of flexibility in the command system that allows rapid evolution of behaviors. Thus, the present study not only shows how segment-specific motor command is established along the

A-P axis during development, but also reveals a potential molecular mechanism that allows for the evolution of the command system. Since regulation of A-P axon guidance by Wnt/Fz-signaling is conserved across phyla, the present study provides a potentially universal principle for the formation and diversification of the command system in the nerve cord.

Limitations of the study

One limitation of this study is that the sample sizes of single-Wave analyses are not high. While clonal analysis has been used to examine fine morphological abnormalities associated with axon guidance defects (Lacoste et al., 2022; Lin et al., 2022; Seroka and Doe, 2019; Xie et al., 2019), these studies were mostly qualitative. This was because the "hit rate" is generally low in this stochastic labelling method. The analyses performed in this work is even more difficult since we have to study single Wave neurons in specific neuromeres. It is a huge challenge to acquire a large number of replicates for neurite quantification.

Although we observed similar axon phenotypes in *DWnt4* mutant and *DFz2/DFz4* KD, it remains to be determined if these proteins interact directly to mediate Wave axon guidance.

In the *DFz2* KD, we observed presynaptic varicosities *en route* of the Wave axon extending posteriorly (Figures 1D and E), but whether there are functional synapses in this region and what are the ectopic synaptic partners remain to be explored. This would be an interesting approach to identify the neurons that initiate forward locomotion in the posterior VNC, where forward locomotion is usually initiated.

Finally, the gradient of the DFz2 expression (Figure 4E) was weak and needs to be validated further by using more specific antibodies. Furthermore, it is crucial to study if DFz2 expression in Wave neurons is graded along the A-P axis.

Acknowledgement

We would like to thank Shoya Ohura and Sawako Niki for the help in screening, Hiroshi Kohsaka for sharing the code for behavior analysis, James Truman for providing reagent identifier, and Matthias Landgraf for sharing unpublished observations. We thank Richard Benton and Michael P. Shahandeh for comments on the manuscript.

We would also like to thank Gimena Alegre, Vivian Budnik, Andrea Brand, Tzumin Lee, Makoto Sato, Tetsuya Tabata, Travis Thomson, Bloomington Drosophila Stock Center, Vienna Drosophila Resource Center, Developmental Studies Hybridoma Bank, FlyORF team, and KYORIN-Fly for providing reagents. This work was supported by MEXT/JSPS KAKENHI grants (15H04255, 18H05113, 19H04742, 20H05048, 21H02576, 21H05675, 22H05487, 22K19479 to A.N.; 18J10483 to S.Takagi).

Author contributions

S.Takagi and A.N. conceived the project. Experimental contributions were as follows: S.Takagi (Figures 1, 2, 3A-C, 4A-B, S1, S2A-E, S3, S5), S.Takano (Figures 5, S2F and F'), Y.H. (Figures S2G and G'), S.M. (Figures 3D-G and 6), X.Z. (Figure 5), A.N. (Figures 4C-F and S4).

S.Takagi and A.N. wrote the paper with inputs from all the other authors.

Declaration of interests

The authors declare no competing interests.

Figure legends

Figure 1. DFz2 inhibits Wave axon extension towards the posterior end (see also Figures S1-S3)

(A, A') Schematic diagram of Wave neuron morphology and function. Wave neurons are segmentally repeated in the VNC, receive inputs from tactile sensory neurons, and drive distinct behaviors depending on the segment. The anterior Wave (a-Wave) comprises anteriorly polarized axon/dendrite and drive backward locomotion, whereas posterior Wave (p-Wave) has axon/dendrite extension towards the posterior end and drive forward locomotion. (B-E) Lateral view of single-cell images of Wave neurons revealed by mosaic analyses in 3rd instar larvae. The green channel shows Wave neurons, and the blue channel shows anti-HRP staining that visualizes the neuropil. SEZ: subesophageal zone, T1-3: thoracic VNC, A1-8/9: abdominal VNC. (B, C) Control A2 (B) and A6 (C) Wave neuron. Scale bar = 50 µm. White arrows indicate axon processes. (D, E) A2 (D) and A6 (E) Wave neuron in which *DFz2* is knocked-down using the TRiP RNAi line. Note the elongation of the axons towards the posterior end (dotted boxes). Orange arrows indicate the putative presynaptic varicosities in the ectopic axons. (F-J) Tiling profile of the axons of A2 to A6 Wave neurons in control and *DFz2* knocked-down animals. *n* indicates the number of neurons. Tiling percentage indicates the fraction of samples in which the Wave axon innervates the corresponding neuromere. (K, L) Quantification of axon extension towards the posterior end in A2 (K) and A6 (L) Wave neuron measured in MCFO images, following KD and overexpression of *DFz2*, respectively. **: $p <$

0.01, ***: $p < 0.001$, Welch's *t*-test with Bonferroni correction. (M) Summary of *DFz2* KD and overexpression phenotypes.

Figure 2. DFz4 specifically promotes axon extension towards the posterior end in A6-Wave (see also Figure S1-S2)

(A, B) *DFz4* KD A2 (A) and A6 (B) Wave neuron using the TRiP RNAi line. Note the shortening of A6 axon towards the posterior end (dotted box in B, see Figures 1B and C for control). Scale bar = 50 µm. (C-G) Tiling profile of A2 to A6 Wave axons in control and *DFz4* knocked-down animals. *n* indicates the number of neurons. Tiling percentage indicate the fraction of samples (single Wave neurons) whose Wave axon innervated the corresponding neuromere. The same analyses as in Figure 1F-J but for *DFz4* knocked-down animals. The control data in Figures 1F-J are shown as references. (H, I) Quantification of axon extension towards the posterior end in A2 (H) and A6 Wave (I) measured in MCFO images, following KD and overexpression of *DFz4*, respectively. *: $p < 0.05$, Welch's *t*-test with Bonferroni correction. The control data shown in Figures 1K and L are reused for this analysis. (J) Summary of *DFz4* KD and overexpression phenotypes.

Figure 3. DWnt4 regulates A-P extension of Wave axons

(A-C) DWnt4 promotes posterior axon extension of p-Wave. (A, B) Examples of axon morphologies towards the posterior end (white arrows) in control (A) and $DWnt4^{C1/EMS23}$ mutant (B) animals. The posterior end of the axon, derived from p-Wave, is shortened in *DWnt4* mutant. Dotted boxes indicate the abnormal shortening of the axon. (C) Quantification of A6-Wave axon extension to segment A6 or A7. $n = 6$ (control) and 3 ($DWnt4^{C1/EMS23}$) neurons, respectively: $p = 0.0119$, Fisher's exact test. (D-G) DWnt4 regulates axon extension of a-Wave. (D) A2-Wave in

DWnt4$^{C1/EMS23}$ is visualized using heat-shock FlpOut. Note the elongation of its axon towards the posterior end, as well as the shortening of its axon towards the anterior end (dotted boxes). Scale bar = 50 µm. See Figure 1B for control. (E) Tiling profile of A2-Wave axons in control and *DWnt4*$^{C1/EMS23}$ mutant animals. *n* indicates the number of neurons. Tiling percentage indicates the fraction of samples (single Wave neurons) whose Wave axon innervated the corresponding neuromere. The control data in Figure 1F are shown as references. (F, G) Quantification of the relative length (see Method details) of the anterior and posterior fraction of A2-Wave axons between control (visualized by MCFO) and mutant (visualized by heat-shock FlpOut) animals. (F) Quantification of the anterior fraction of A2-Wave axons. (G) Quantification of the posterior fraction of A2-Wave axons. *n* indicates the number of neurons. *: $p < 0.05$, **: $p < 0.01$, Welch's *t*-test. The control data are replotted from Figure 1K for different comparisons. (H) Summary of *DWnt4* phenotypes.

Figure 4. Complementary graded expression of DWnt4 and DFz2 along the A-P axis (see also Figure S4)

(A, B) DWnt4-GFP cells in the embryonic CNS. (A) Distribution of DWnt4-GFP cells. Nuclear-localized GFP is expressed under the regulation *Wnt4*$^{MI03717\text{-}Trojan\text{-}GAL4}$. anti-Elav counterstaining was performed to label all neurons and normalize the GFP signal. GFP expression is stronger in posterior than anterior VNC. Scale bar = 50 µm. (B) Quantification of normalized GFP signals with respect to Elav signals in each neuromere (where 1 denotes the maximum). $n = 5$ animals. Not having a common alphabet indicated above the plots between groups indicates statistical significance (α=0.05, Tukey's HSD test).

(C, D) Expression of DWnt4 protein in the neuropil of each neuromere. (C) DWnt4 and HRP immunostaining. Scale bar = 10 µm. (D) Normalized DWnt4/HRP signals in each neuromere

are calculated. n = 18 samples from 9 animals *: $p < 0.05$, ***: $p < 0.001$, paired t-test (comparison to A8).

(E, F) Expression of DFz2 protein in the neuropil of each neuromere. (E) DFz2 and HRP immunostaining. Scale bar = 10 μm. (F) Normalized DFz2/HRP signal in each neuromere are calculated. n = 16 samples from 8 animals *: $p < 0.05$, **: $p < 0.01$, paired t-test (comparison to A2).

(G) Model of segment-specific axon guidance in Wave neurons. DWnt4 serves as a graded axon guidance cue (concentrated towards the posterior end of VNC) and is recognized by DFz2/DFz4 receptors as repulsive/attractive cue, respectively. DFz2 functions both in a-Wave and p-Wave, whereas DFz4 functions selectively in p-Wave.

Figure 5. *DFz2* KD switches the motor commands of a-Wave neurons (see also Figure S5)

(A) Schematic of area-confined optogenetics in *ex vivo* central nervous system. (B, C) Examples of fictive backward and forward locomotion activity patterns of motor neurons induced by a-Wave neuron stimulation in wild-type (B) and *DFz2*-KD [KK] (C) animals, respectively. Top row: calcium imaging of motor neurons visualized by *tub-LexA* > RGECO-1. Images of three different timings (in the order of red, green, and blue) are superimposed. Propagation of motor activity from anterior to posterior segments (B) indicates backward wave, whereas activity in the opposite direction (C) indicates forward wave. Bottom row: exemplary calcium traces of motor neuron activity in segments A5-A7. Blue bars indicate the timing of stimulation. (D-G) Quantifications of the number of backward and forward waves upon anterior/posterior stimulation of Wave neurons. Control: *tub-LexA/(+/Y); UAS-ChR2^{T159C}/+; LexAop-RGECO-1/R60G09-GAL4, UAS-CD4-tdGFP, DFz2* KD: *tub-LexA/(+/Y);*

UAS-ChR2^{T159C}/ UAS-DFz2-RNAi[KK]; LexAop-RGECO-1/R60G09-GAL4, UAS-CD4-tdGFP. (D) Backward waves in response to anterior stimulation. (E) Forward waves in response to anterior stimulation. (F) Backward waves in response to posterior stimulation. (G) Forward waves in response to posterior stimulation. *: $p < 0.05$, n.s., not significant. Mann-Whitney's *U*-test.

<u>Figure 6. Modulation of tactile-evoked behavior by *DFz2* KD in Wave neurons</u>

(A) Left panel: Scheme of gentle-touch assay using von Frey filament. Right panel: Stereotypic behavioral responses induced by the gentle head touch, categorized according to the Kernan score (Kernan et al., 1994). (B-C") Alteration in behavior responses upon *DFz2* KD using UAS-*DFz2-RNAi* [KK] (B-B'') or UAS-*DFz2-RNAi* [GD] (C-C''). (B, C) Distribution of the Kernan score. Driver control; *R60G09-GAL4/+*, effector control; UAS-*DFz2-RNAi/+*, and experimental group (*R60G09-GAL4* > UAS-*DFz2-RNAi*). n = 40 trials each. (B', C') Fraction of behavioral responses classified as backward (scores 3 and 4) and turning (score 2). The numbers indicate the trials that induced the classified response. *: $p < 0.05$, **: $p < 0.01$, ***: $p < 0.001$, Fisher's exact test with Bonferroni correction. (B'', C'') Quantifications of stride duration of forward locomotion following gentle touch. Note that smaller stride duration indicates faster forward locomotion. n =36 (driver control), 40 (effector control), 39 (B'') and 40 (C'') (experimental) trials. *: $p < 0.05$, ***: $p < 0.001$, Steel-Dwass test. (D) Summary of the current study.

Materials and methods

RESOURCE AVAILABILITY

• Lead contact

Further information and requests for resources should be directed to A.N. (nose@k.u-tokyo.ac.jp).

• Materials availability

This study did not generate any new reagents.

• Data and code availability

Raw data and analysis codes that are used for the present study will be made available for public download as of the date of publication (https://data.mendeley.com/datasets/66jh2hxz2w/draft?a=f4557904-a446-4786-a978-cdd1c2eab7b4; DOI: 10.17632/66jh2hxz2w.1). Confocal images, calcium imaging videos, and behavioral videos are shared upon request.

EXPERIMENTAL MODEL AND SUBJECT DETAILS

Drosophila melanogaster strains

The following fly strains were used in this study.

•*yw* (Bloomington *Drosophila* Stock Center, #6598)

•*DWnt4*^{C1} (Null allele of *DWnt4* (Cohen et al., 2002), Bloomington *Drosophila* Stock Center, #6651)

•*DWnt4*^{EMS23} (Null allele of DWnt4 (Cohen et al., 2002), Kyoto Stock Center, #108-974)

•*DWnt5*^{400} (Null allele of *DWnt5* (Fradkin et al., 2004). Bloomington *Drosophila* Stock Center, #64300)

•*DWnt6*^{KO} (Deletion of exon 1 of *DWnt6* (Doumpas et al., 2013), Bloomington *Drosophila* Stock Center, #76311)

•*DWnt8*^{KO1} (Knock-out allele of *DWnt8* (a.k.a. *wntD*(Gordon et al., 2005), Bloomington *Drosophila* Stock Center, #38407)

•UAS-*CD4-tdGFP* (A membrane-fused GFP, Bloomington *Drosophila* Stock Center, #35836)

•UAS-*CD4::GCaMP6f* (A membrane-fused GCaMP, Takagi et al., 2017)

•*R57C10-FlpL;;pJFRC201*-10XUAS-FRT > STOP > FRT-*myr::smGFP-HA, pJFRC240*-10XUASFRT > STOP > FRT- *myr::smGFP-V5-THS*-10XUAS-FRT > STOP > FRT-*myr::smGFP-FLAG, pJFRC210*-10XUAS-FRT > STOP > FRT-*myr::smGFP-OLLAS* (Named shortly as MCFO-6 in (Nern et al., 2015). Bloomington *Drosophila* Stock Center (#64090), RRID: BDSC_64090)

•20XUAS > dsFRT > -*CsChrimson::mVenus (attP18), pBPhsFlp2::Pest (attP3)*; Express CsChrimson::mVenus under GAL4 control when the STOP cassette is removed by hsFlp2, a heat-shock-dependent recombinase that targets FRT, Takagi et al., 2017)

•*MB120B-spGAL4* (A combination of GAL4.AD and GAL4.DBD that specifically targets Wave neurons, Takagi et al., 2017)

•*R60G09-GAL4* (A GAL4 line that targets Wave neurons mainly in neuromeres A2-A6. Identified through visual screening of 6849 GAL4 driver lines registered in the FlyLight

database (Li et al., 2014; Manning et al., 2012). Bloomington Drosophila Stock Center (#46441))

•*R77H11-GAL4* (A GAL4 line that targets Wave neurons mainly in neuromeres A1-A6. Described in Masson et al., 2020. Bloomington Drosophila Stock Center (#39983))

•*R77H11-LexA* (A LexA version of *R77H11* enhancer used for double labelling with *MB120B-spGAL4* and *R60G09-GAL4*. Bloomington Drosophila Stock Center (#54720))

• $Wnt4^{MI03717\text{-}Trojan\text{-}GAL4}$ (A GAL4 insertion near the Wnt4 locus by MiMIC cassette recombination. Bloomington Drosophila Stock Center (#67449), RRID: BDSC_67449)

•*tub-LexA* (Targets all cell (Lai and Lee, 2006). Used to image motor neuron activity in *ex vivo* preparation. Gift from Dr. Tzumin Lee)

• $elav\text{-}GAL4^{3E1}$ (Targets all neurons. Used to knock down *DFz2* in all neurons. Davis et al., 1997)

•UAS-*mCherry*.VALIUM10 (A control stock for RNAi reporter lines using VALIUM10 or VALIUM20 vectors. Generated by the Transgenic RNAi Project (TRiP), Bloomington *Drosophila* Stock Center, #35787, RRID: BDSC_35787)

•UAS-*DFz*-RNAi (An RNAi reporter line used to knock down DFz. Generated by the Transgenic RNAi Project (TRiP), Bloomington *Drosophila* Stock Center, #34321, RRID: BDSC_34321)

•UAS-*DFz2*-RNAi (An RNAi reporter line used to knock down DFz2. Generated by the Transgenic RNAi Project (TRiP), Bloomington *Drosophila* Stock Center, #67863, RRID: BDSC_67863)

•UAS-*DFz3*-RNAi (An RNAi reporter line used to knock down DFz3. Generated by the Transgenic RNAi Project (TRiP), Bloomington *Drosophila* Stock Center, #44468, RRID: BDSC_44468)

•UAS-*DFz4*-RNAi (An RNAi reporter line used to knock down DFz4. Generated by the Transgenic RNAi Project (TRiP), Bloomington *Drosophila* Stock Center, #64990, RRID: BDSC_64990)

•UAS-*drl*-RNAi (An RNAi reporter line used to knock down Drl. Generated by the Transgenic RNAi Project (TRiP), Bloomington *Drosophila* Stock Center, #39002, RRID: BDSC_39002)

•UAS-*Drl-2*-RNAi [TRiP] (An RNAi reporter line used to knock down Drl-2. Generated by the Transgenic RNAi Project (TRiP), Bloomington *Drosophila* Stock Center, #55893, RRID: BDSC_55893)

•UAS-*Drl-2*-RNAi [KK] (An RNAi reporter line used to knock down Drl-2. Generated by the VDRC genome-wide Drosophila RNAi project, Vienna *Drosophila* Resource Center, #102192)

•UAS-*smo*-RNAi (An RNAi reporter line used to knock down Smo. Generated by the Transgenic RNAi Project (TRiP), Bloomington *Drosophila* Stock Center, #43134, RRID: BDSC_43134)

•UAS-*Corin*-RNAi (An RNAi reporter line used to knock down Corin. Generated by the Transgenic RNAi Project (TRiP), Bloomington *Drosophila* Stock Center, #41721, RRID: BDSC_41721)

•UAS-*DFz2*-RNAi [GD] (An alternative RNAi reporter line used to knock down DFz2. Included in the GD collection (P-element) generated by the VDRC genome-wide Drosophila RNAi resource. VDRC #44390)

•UAS-*DFz2*-RNAi [KK] (An alternative RNAi reporter line used to knock down DFz2. Included in the KK collection (phiC31) generated by the VDRC genome-wide Drosophila RNAi resource. VDRC #108998)

•UAS-*DFz4*-RNAi [KK] (An alternative RNAi reporter line used to knock down DFz4. Included in the KK collection (phiC31) generated by the VDRC genome-wide Drosophila RNAi resource. VDRC #102339)

•UAS-*DFz2*-ORF (An ORF reporter line used for ectopic/overexpression of DFz2. Generated by the Zurich ORFeome Project, FlyORF, #F001187)

•UAS-*DFz4*-ORF (An ORF reporter line used for ectopic/overexpression of DFz4. Generated by the Zurich ORFeome Project, FlyORF, #F001662)

• UAS-$ChR2^{T159C}$ (A Channelrhodopsin variant (Berndt et al., 2011), transgenic flies generated as described in Fushiki et al., 2016)

• LexAop-*R-GECO-1* (A red-shifted genetically encoded calcium indicator (GECI), (Kohsaka et al., 2014, Zhao et al., 2011))

METHOD DETAILS

Immunohistochemistry

Immunohistochemistry experiments for 3rd instar larvae were performed as done previously (Takagi et al., 2017).

For 12-16hAEL embryos in Figure S1B and C, whole-mount staining was performed. First, the animals were chemically dechorionated with 50% sodium hypochlorite solution, transferred into a glass vial containing 2 mL heptane (organic layer), and were fixed by 2 mL addition of 4% paraformaldehyde in PBS (water layer) for 30 min at room temperature with shaking. After removal of the water layer, half of the heptane was removed and 1 mL MeOH was added. The vial was vigorously shaken for 20 sec to facilitate cracking of the vitelline membrane. After removing the organic layer, the embryos were washed with MeOH twice, and with EtOH once. The embryos were then transferred into a plastic microtube, and thereafter the same protocol as in the larvae was applied.

For late-stage embryos in Figures 4, S1D, and S4, dissection was performed to increase staining efficacy. The dissection was performed by gluing the animal onto double-sided scotch tape and opening the dorsal part using a sharp needle.

The laser intensities used to quantify DWnt4 and DFz2 signals in Figure S4 were kept the same between control and mutant embryos for each group.

The list of the antibodies and the dilution is as follows:

•rabbit anti-GFP (Af2020, Frontier Institute; 1:1000; RRID: AB 10615238)

•mouse anti-Fas2 (1D4, Hybridoma Bank (University of Iowa); 1:10; RRID: AB 528235)

•rat anti-Elav (7E8A10, Hybridoma Bank (University of Iowa); 1:10; RRID: AB 528218)

•guinea pig anti-GFP (Af1180, Frontier Institute; 1:1000; RRID: AB 2571575)

•rabbit anti-HA (C29F4, Cell Signaling Technology; 1:1000; RRID: AB 1549585)

•mouse anti-V5 (R960-25, Invitrogen; 1:500; RRID: AB 2556564)

•rabbit anti-DWnt4 (Cohen et al., 2002; 1:100; kindly provided by M. Sato)

•rabbit anti-DFz2 (Packard et al., 2002; 1:100; kindly provided by G. Alegre, V. Budnik, and T. Thomson)

•goat Alexa Fluor 488 or Cy3-conjugated anti-rabbit IgG (A-11034 or A-10520, Invitrogen Molecular Probes; 1:300; RRID: AB 2576217 or AB 10563288)

•goat Alexa Fluor 555 or Cy5-conjugated anti-mouse IgG (A-21424 or A-10524, Invitrogen Molecular Probes; 1:300; RRID: AB 141780 or AB 2534033)

•goat Cy5-conjugated anti-HRP (123-175-021, 1:300, Jackson ImmunoResearch Laboratories Inc.)

•Alexa Fluor 647 AffiniPure Goat Anti-Horseradish Peroxidase (123-605-021, 1:300, Jackson ImmunoResearch Laboratories Inc., RRID: AB_2338967)

Samples of poor quality (due to damage during dissection and/or drift during confocal imaging) were excluded from further analyses.

Staging of embryos

Female and male flies of appropriate genotypes were kept in a vial for more than one day to allow copulation. The eggs were collected by trapping the parent flies on a yeast paste-coated apple plate, covered with a cup with small air holes. To prevent collecting withheld eggs (which are most likely pre-developed), the flies were allowed to lay their eggs on the plate for one hour. For experiments in Figure S1, we adopted the following procedure. The flies were transferred onto another fresh plate and were allowed to lay eggs for one hour. The plates were kept at 25°C until the embryos developed to the desired stage. The stages are indicated as hours after egg laying (hAEL), which includes an error of ±0.5 hours. The stages were further validated at the time of confocal imaging by observing the development of the gut (Campos-Ortega and Hartenstein, 1985), and animals that did not meet the standard were excluded.

For experiments in Figures 4 and S4, the flies were transferred onto a fresh plate and were allowed to lay eggs for 18-24 hrs at 25°C. The stage (Stage 16) was confirmed by the development of the gut.

Identification and characterization of *R60G09-GAL4* and embryonic Wave neurons

Since neurite outgrowth of larval neurons occurs during embryogenesis, we first searched for a GAL4 line that targets Wave neurons consistently from embryonic to larval stages, as the previously used GAL4 (*MB120B-spGAL4*) lacks expression at embryonic stages (animals with GFP-positive cells: n = 2 out of 70 animals). We identified in the FlyLight database a sparse GAL4 line, *R60G09-GAL4*, which targets Wave neurons in 3rd instar larvae (Figure S1E) with the exception of a single pair of ascending neurons in T2 in the VNC, and also drives expression in two pairs of segmental neurons in the embryo (Figures S1B and C). Stage-by-stage

observation revealed that one of the GAL4-targeted embryonic neurons is a Wave neuron, which was continuously marked and thus can be traced through embryonic stages (10, 12, 16, 18, and 20 hAEL; Figures S1B, C, and D) to larval stages (3rd instar; Figures S1E). Another *GAL4*-targeted non-Wave neurons (that resides posteriorly to Wave with the cell size being larger) started to get fragmented and densely stained in 16hAEL (Figure S1C) and was extinct at later stages (Figures S1D and E) in segments anterior than A5, suggesting that this neuron is dMP2 (Miguel-Aliaga, 2004; Miguel-Aliaga et al., 2008). Although dMP2 neurons in segments A6-A8 survived up to larval stages, the GAL4-driven expression in dMP2 neurons vanished in these stages (Figure S1E).

Primary RNAi/mutant tests

To visualize the Wave neurites, membrane-bound reporters (CD4-tdGFP or CD4-GCaMP6f, with the latter being brighter when stained) were expressed. The CNS was stained by anti-GFP and anti-Fas2 antibodies. Confocal stack images of the CNS were taken by using a confocal microscope (FV1000, Olympus).

For RNAi-based KD experiments (Figure S2D), female UAS-RNAi flies were crossed to *R60G09-GAL4. UAS-CD4-GCaMP6f* males and the larvae of the next generation were examined. The nine genes tested are known guidance cue receptors possibly involved in Wnt signaling: *DFz, DFz2, DFz3, DFz4, drl, Drl-2, smo,* and *Corin*. All the RNAi lines used here are from the Transgenic RNAi Project (TRiP), except for *Drl-2* where TRiP was used for one sample and KK line for the other three.

For mutant-based knock-out experiments (Figure S2E), *R77H11-GAL4, UAS-CD4-GCaMP6f* (or *MB120B-spGAL4, UAS-CD4-GCaMP6f* for *DWnt5* mutants) flies were used since the expression was nicely confined to Wave neurons (Masson et al., 2020).

Single-Wave labelling by heat-shock FlpOut (Figures S3D-G)

Female *20XUAS > dsFRT > -CsChrimson::mVenus, pBPhsFlp2::Pest; DWnt4*^{EMS23} flies were crossed to *DWnt4*^{C1}; *R77H11-GAL4* males and housed in tubes with fly food. The tubes containing eggs and 1st-2nd instar larvae were placed into an incubator set to 37.5-38.7 °C for 1 hr. The tubes were put back to 25°C to raise the eggs up to the 3rd instar larvae. The CNS was dissected and Wave neurons were visualized by staining mVenus with anti-GFP antibody. The segment identities of Wave neurons were determined by observing the entry point of the neurite from the soma, based on anti-HRP staining.

Area-confined optogenetics *ex vivo* (Figure 5)

The procedure was in accord with our previous work (Takagi et al., 2017). *R60G09-GAL4, UAS-CD4-tdGFP* or UAS-*DFz2-RNAi [KK]*; *R60G09-GAL4, UAS-CD4-tdGFP* female flies were crossed to *tub-LexA*; *UAS-ChR2*^{T159C}; *LexAop-RGECO-1* male flies. The larvae of the next generation were grown at 25°C. First or second instar larvae were picked, gently washed, and transferred onto an apple-juice agar plate coated with yeast paste containing 10 mM ATR. The plate was covered with the plastic cover and aluminum foil, placed in 25°C for two nights. The larvae were dissected on a syligard-coated dish in TES buffered solution (TES 5 mM, NaCl 135

mM, KCl 5 mM, $MgCl_2$ 4 mM, $CaCl_2$ 2 mM, sucrose 36 mM, pH = 7.15). The CNS of the larva was isolated from the body wall and set on a MAS-coated slide glass (S11215, Matsunami Glass Ind.), and the buffered solution was refreshed before the sample was set under the stereomicroscope (FV1000, Olympus).

The microscope was set-up with two optical paths: one for area-confined stimulation and the other for calcium imaging. The two paths were isolated by using a dichroic mirror (ADM 405/488, Olympus). The isolated CNS was placed under a water immersion lens (20x, XLUMPLFLN, NA1.0, WD 2 mm, Olympus). Fluorescence derived from the YFP tagged to the $ChR2^{T159C}$ protein was scanned using a 515nm Ar laser, to confirm the expression of $ChR2^{T159}$ in the GAL4-expressing cells. For image acquisition, the attached software (Olympus FLUOVIEW Ver.4.2) was used.

The stimulation was achieved using a 488nm Ar laser, which can be confined to ~50 μm in diameter (based on the illuminated region in the imaging video). The intensity of stimulation was set to 8.3 μW. Concurrently with the stimulation, calcium imaging was done by expressing RGECO (Zhao et al., 2011), a class of red-shifted GECI, under the regulation of *tub-LexA* to enable pan-neuronal imaging. The imaging was achieved by recording the fluorescence with an EMCCD camera (iXon3, ANDOR TECHNOLOGY). The pump light for imaging was derived from a Xe lamp (X-Cite, Excelitas Technologies).

The stimulation sites were determined based on the segmental motor neurons evident in the RGECO image. Segments A1 (for a-Wave) and A5 (for p-Wave) were selected since *DFz2* KD did not impair the innervation of a-Wave and p-Wave axons in these regions respectively. Each stimulation lasted for 5 secs with > 20 sec intervals. The stimulation was performed 3 times each for 19 (control) and 17 (*DFz2* KD) animals.

The motor outputs were monitored by imaging the RGECO fluorescence, in the region of the dorsal neuropile where the motoneurons dendrites are concentrated. The motoneurons dendrites are clustered in each neuromere, thus it is possible to distinguish the activity of the motoneurons from one neuromere to another.

Optogenetics (with CsChrimson) in free-moving larvae (Figure S5)

UAS-CsChrimson female flies were crossed to *R60G09-GAL4* or *UAS-DFz2-RNAi [TRiP]; R60G09-GAL4* males. The larvae from the next generation were grown at 25°C. 2nd or 3rd instar larvae were picked, gently washed, and transferred onto an apple-juice agar plate coated with yeast paste, either containing 2 mM of all-trans retinal (ATR) or none (ATR concentration was calculated based on the volume of the dry yeast. Note that the same amount of distilled water was added to make yeast paste). The plate was covered with the plastic cover and aluminum foil and placed at 25°C for one night. The behavioral experiment was conducted on an apple juice agar plate, which was placed on a heating plate to set the surface temperature of the agar within 25°C ± 1°C. The larvae were placed on the fresh apple-plate for over 5 min before the behavioral assays. 660 nm LED light at the density of 20~25 μW/mm^2 (THORLABS) was used for the stimulation of CsChrimson. The stimulation trials were delivered twice for each animal, with a duration of 10-15 s for each trial, and > 15 s intervals between each trial. Video recording was conducted under a stereomicroscope (SZX16, Olympus), while the background illumination was minimized so as not to activate CsChrimson.

Gentle touch assay (Figures 6)

The behavioral experiment was conducted on an apple juice agar plate, which was placed on a heating plate to set the surface temperature of the agar within 25°C ± 1°C. von Frey filament (Touch Test Sensory Evaluator (0.07 g), North Coast; #NC12775-04) was used to provide gentle head touch. Gentle touch was applied to the target site (dorsal side of T3 ± 1 segment) until the filament showed a mild bend, so that a consistent force was applied across trials. Trials with failed stimulation (wrong location, insufficient filament bend) were excluded from the analyses. Five trials were performed for eight animals in each group. The experiment was performed by mixing the identities of genetic groups to make their identities blind to the examiner. The genotypes are as follows: driver control (*yw* × *R60G09-GAL4*), TRiP effector control (*yw* × *UAS-DFz2-RNAi*[TRiP]), KK effector control (*yw* × UAS-*DFz2-RNAi*[KK]), GD effector control (*yw* × UAS-*DFz2-RNAi*[GD]), TRiP experimental (UAS-*DFz2-RNAi*[TRiP] × *R60G09-GAL4*), KK experimental (UAS-*DFz2-RNAi*[KK] × *R60G09-GAL4*), GD experimental (UAS-*DFz2-RNAi*[TRiP] × *R60G09-GAL4*).

QUANTIFICATION AND STATISTICAL ANALYSIS

Primary RNAi/mutant test (Figure S2)

The projection of Wave axons was manually examined with Fas2 reference as follows. For an axon, as it runs dorsally, one of the Fas2 tract TP1 was considered as a boundary (Landgraf et al., 2003a). The neuromere identity was determined starting from T3, where Fas2 tracts are uniquely identifiable. For analysis in Figure S2G and G', HRP staining was used as a reference and hence the criteria used was the same as in the clonal analysis (described below).

For examination of the Wave axon/dendrite projection region, three animals were examined for each RNAi strain. If GFP expression was not obtained for more than three neurons (due to GAL4 expression stochasticity), we added three to six animals until the sample size reached three.

Clonal analyses (Figures 1, 2, 3, S2, and S3)

Wave neurites were visualized by anti-V5/anti-HA (for MCFO) or by anti-GFP (for heat-shock FlpOut) antibody staining with the anti-HRP staining as a reference, which clearly stains the anterior commissure (AC) and posterior commissure (PC) in each neuromere. The segment identity was assigned starting from T3 which is uniquely identifiable. The boundary between neuromeres A_k and A_{k+1} (k=1, 2, …, 7) is approximately the center line between the PC in neuromere A_k and AC in neuromere A_{k+1} (Landgraf et al., 2003b). The presence of a neurite in a specific neuromere was determined as follows. For anterior projection, when the neurite

crossed the PC in neuromere A_k, it was counted as being present in A_k. For posterior projection, when the neurite crossed the AC in neuromere A_k, it was counted as being present in A_k. These definitions were intended to exclude vague projections into a neuromere. Quantification of relative axon length is described in the following section.

Quantification of relative axon length (Figures 1, 2, 3, and S2)

The relative position c $(0 \leq c < 1)$ of the axon landmarks (axon branching point, anterior end, and posterior end) was calculated as follows.

$$c(x, y) = \frac{(x_1 - x_0)(x - x_0) + (y_1 - y_0)(y - y_0)}{(x_1 - x_0)^2 + (y_1 - y_0)^2}$$

where point (x, y) denotes the pixel coordinate of a specific point in a confocal stack image taken from the dorsal side. The points of interest are:

(x, y): axon branching point, anterior end, or posterior end

(x_0, y_0): the anterior segmental border (calculated as the midpoint of the center of the dorsal posterior commissure (dPC) of the prior neuromere and the center of the dorsal anterior commissure (dAC) of the present neuromere, derived from anti-HRP staining)

(x_1, y_1): the posterior segmental border (calculated as the midpoint of the center of the dPC of the present neuromere and the center of the dAC of the next neuromere, derived from anti-HRP staining).

By adding relative position c to the neuromere identity n $(n = 1, 2, \ldots, 11$ for neuromeres T1, T2, T3, A1, …, A8), normalized landmark positions $\hat{c}(x, y) = c(x, y) + n(x, y)$ were defined and their distances were used to calculate relative axon lengths.

As relative positions of landmarks are critical for these analyses, images with drifts and/or perturbation were excluded.

Quantification of DWnt4/DFz2 expression (Figures 4 and S4)

To quantify the florescence from immunohistochemistry images, ROIs were set to each hemisegment to calculate the mean intensity. The segment identity was assigned for each block of anterior and posterior commissures (AC and PC) in the neuropil starting from A8 (in embryos) or A1 (in larvae).

To quantify the anti-DWnt4 and anti-DFz2 signals, Z-stack images that extracted the maximum intensity pixels within the neuropil in each hemisegment were used. ROIs were set as circles that cover the lateral neurite-dense regions in left and right hemisegments. The signals from anti-DWnt4/DFz2 were normalized by the anti-HRP signals in the corresponding ROIs. Neuromere A1 was excluded from the analysis as many images did not cover this region. Samples with ambiguous A-P directionality were also excluded.

To quantify the GFP.nls and anti-Elav signals in embryos, the ROIs were set as polygons (drawn based on the anti-Elav image) that encircled the segmental bumps at the lateral edge and imaginary boundaries between segments (that appeared as arc-shaped dark ditches). Since the boundary was less evident posterior than A8, all the terminal segments were included and named as “A8/9”.

Quantification of fictive locomotion in area-confined optogenetics *ex vivo* (Figure 5)

We defined a forward wave as a bilateral and sequential motor activity propagating from posterior to anterior segments, and a backward wave as that in the opposite direction, in more than three consecutive abdominal segments. The waves that emerged before and after the stimulus onset were not taken into account. Stimulation epochs where no evoked/spontaneous motor waves were observed afterwards were excluded from the analyses, as the sample quality may be severely impaired. Off-targeted, severely distorted, and/or low fluorescent samples were also excluded. Two independent analyses were performed (by S.Takagi and S.Takano) and we confirmed that a consistent conclusion was obtained.

Quantification of larval behaviors (Figures 6 and S5)

Larval behaviors were manually quantified. Larval locomotion was counted when a complete sequence of muscle contraction across all segments was observed, with the direction from anterior to posterior being backward locomotion and the other way around being forward locomotion (Berni et al., 2012). Rolling was defined as a 360-degree rolling of larval body to the lateral direction.

In quantification of larval behaviors upon optogenetic stimulation (Figure S5), the first 10 secs just prior to and after stimulation onset in each trial was used (to avoid the effect of desensitization) and then summed across trials.

In quantification of stride durations (Figures 6 and S5), the duration between the start (landing of the posterior end of the larval body) and the end (landing of the anterior end of the larval body) of forward locomotion that occurred just prior to and after the first stimulation onset (Figure S5) or just after each gentle touch (Figure 6) was measured. In Figure 6, the trials

where the larvae were outside the field of view when performing forward locomotion following the stimulus were excluded from the analyses.

In quantification of behaviors upon gentle touch (Figure 6), the Kernan scoring was performed by manually observing the recorded video. To minimize scoring bias, two independent analyses were performed (by S. M. and S. Takagi) and we confirmed that a consistent conclusion was obtained.

Statistical analyses

All statistical tests were performed using R-project (http://www.r-project.org). The statistical tests used are indicated in the respective figure legends or in the text.

In the primary RNAi analysis and the mutant analysis, the Chi-square test followed by Haberman's adjusted residual analysis (Haberman, 1973) was applied to determine the statistical significance of each cell in the cross-classified table. To avoid multiple comparison problems, adjusted significance level was calculated in accord with Sidak, 1967, as is recommended in Beasley and Schumacker, 1995, as follows:

$$\alpha_{adjusted} = 1 - (1 - \alpha)^{\frac{1}{k}}$$

where *k* denotes the number of cells in the table. Here, we set $\alpha = 0.05$.

Supplemental items

Figure S1. *R60G09-GAL4* consistently targets Wave neurons from embryonic to larval stages (related to Figures 1-3)

Figure S2. Identification of candidate Wnt receptors and ligands that regulate A-P Wave axon guidance (related to Figures 1-3)

Figure S3. Effect of *DFz2* KD on Wave dendrite extension (related to Figure 1)

Figure S4. Expression of DWnt4 and DFz2 is suppressed in mutants (related to Figure 4)

Figure S5. *DFz2* KD in Wave neurons alters motor commands *in vivo* (related to Figure 5)

References

Ardesch, D.J., Scholtens, L.H., Li, L., Preuss, T.M., Rilling, J.K., and Heuvel, M.P. van den (2019). Evolutionary expansion of connectivity between multimodal association areas in the human brain compared with chimpanzees. Proceedings of the National Academy of Sciences *116*, 7101–7106. https://doi.org/10.1073/PNAS.1818512116.

Barthélemy, D., Leblond, H., Provencher, J., and Rossignol, S. (2006). Nonlocomotor and Locomotor Hindlimb Responses Evoked by Electrical Microstimulation of the Lumbar Cord in Spinalized Cats. J Neurophysiol *96*, 3273–3292. https://doi.org/10.1152/jn.00203.2006.

Beasley, T.M., and Schumacker, R.E. (1995). Multiple Regression Approach to Analyzing Contingency Tables: Post Hoc and Planned Comparison Procedures. The Journal of Experimental Education *64*, 79–93. https://doi.org/10.1080/00220973.1995.9943797.

Bekkers, J.M., and Stevens, C.F. (1991). Excitatory and inhibitory autaptic currents in isolated hippocampal neurons maintained in cell culture. Proc Natl Acad Sci U S A *88*, 7834. https://doi.org/10.1073/PNAS.88.17.7834.

Berni, J., Pulver, S.R., Griffith, L.C., and Bate, M. (2012). Autonomous circuitry for substrate exploration in freely moving drosophila larvae. Current Biology *22*, 1861–1870. https://doi.org/10.1016/j.cub.2012.07.048.

Bouvier, J., Caggiano, V., Leiras, R., Caldeira, V., Bellardita, C., Balueva, K., Fuchs, A., and Kiehn, O. (2015). Descending Command Neurons in the Brainstem that Halt Locomotion. Cell *163*, 1191–1203. https://doi.org/10.1016/j.cell.2015.10.074.

Campos-Ortega, J.A., and Hartenstein, V. (1985). The Embryonic Development of Drosophila melanogaster (Berlin, Heidelberg: Springer Berlin Heidelberg).

Cash, S., Chiba, A., and Keshishian, H. (1992). Alternate neuromuscular target selection following the loss of single muscle fibers in Drosophila. Journal of Neuroscience *12*, 2051–2064. https://doi.org/10.1523/JNEUROSCI.12-06-02051.1992.

Chakraborty, M., and Jarvis, E.D. (2015). Brain evolution by brain pathway duplication. Philosophical Transactions of the Royal Society B: Biological Sciences *370*. https://doi.org/10.1098/RSTB.2015.0056.

Cohen, E.D., Mariol, M.-C., Wallace, R.M.H., Weyers, J., Kamberov, Y.G., Pradel, J., and Wilder, E.L. (2002). DWnt4 Regulates Cell Movement and Focal Adhesion Kinase during Drosophila Ovarian Morphogenesis. Dev Cell *2*, 437–448. https://doi.org/10.1016/S1534-5807(02)00142-9.

Davis, G.W., Schuster, C.M., and Goodman, C.S. (1997). Genetic Analysis of the Mechanisms Controlling Target Selection: Target-Derived Fasciclin II Regulates the Pattern of Synapse Formation. Neuron *19*, 561–573. https://doi.org/10.1016/S0896-6273(00)80372-4.

Doumpas, N., J??kely, G., and Teleman, A.A. (2013). Wnt6 is required for maxillary palp formation in Drosophila. BMC Biol *11*. https://doi.org/10.1186/1741-7007-11-104.

Eschbach, C., and Zlatic, M. (2020). Useful road maps: studying Drosophila larva's central nervous system with the help of connectomics. Curr Opin Neurobiol *65*, 129–137. https://doi.org/10.1016/J.CONB.2020.09.008.

Faumont, S., Lindsay, T.H., and Lockery, S.R. (2012). Neuronal microcircuits for decision making in C. elegans. Curr Opin Neurobiol *22*, 580–591. https://doi.org/10.1016/j.conb.2012.05.005.

Fradkin, L.G., van Schie, M., Wouda, R.R., de Jong, A., Kamphorst, J.T., Radjkoemar-Bansraj, M., and Noordermeer, J.N. (2004). The Drosophila Wnt5 protein mediates selective axon fasciculation in the embryonic central nervous system. Dev Biol *272*, 362–375. https://doi.org/10.1016/J.YDBIO.2004.04.034.

Gierer, A. (1987). Directional cues for growing axons forming the retinotectal projection. Development *101*, 479–489. https://doi.org/10.1242/DEV.101.3.479.

Gordon, M.D., Dionne, M.S., Schneider, D.S., and Nusse, R. (2005). WntD is a feedback inhibitor of Dorsal/NF-κB in Drosophila development and immunity. Nature *437*, 746–749. https://doi.org/10.1038/nature04073.

Grillner, S., and Robertson, B. (2016). The Basal Ganglia Over 500 Million Years. Current Biology *26*, R1088–R1100. https://doi.org/10.1016/J.CUB.2016.06.041.

Haberman, S.J. (1973). The Analysis of Residuals in Cross-Classified Tables. Biometrics *29*, 205. https://doi.org/10.2307/2529686.

Hassan, B.A., and Hiesinger, P.R. (2015). Beyond Molecular Codes: Simple Rules to Wire Complex Brains. Cell *163*, 285–291. https://doi.org/10.1016/J.CELL.2015.09.031.

Hessinger, C., Technau, G.M., and Rogulja-Ortmann, A. (2017). The *Drosophila* Hox gene *Ultrabithorax* acts in both muscles and motoneurons to orchestrate formation of specific neuromuscular connections. Development *144*, 139–150.

https://doi.org/10.1242/dev.143875.

Hilliard, M.A., and Bargmann, C.I. (2006). Wnt signals and Frizzled activity orient anterior-posterior axon outgrowth in C. elegans. Dev Cell *10*, 379–390. https://doi.org/10.1016/j.devcel.2006.01.013.

Hu, Y., Wang, C., Yang, L., Pan, G., Liu, H., Yu, G., and Ye, B. (2020). A Neural Basis for Categorizing Sensory Stimuli to Enhance Decision Accuracy. Current Biology *30*, 4896-4909.e6. https://doi.org/10.1016/J.CUB.2020.09.045.

Inaki, M., Yoshikawa, S., Thomas, J.B., Aburatani, H., and Nose, A. (2007). Wnt4 Is a Local Repulsive Cue that Determines Synaptic Target Specificity. Current Biology *17*, 1574–1579. https://doi.org/10.1016/j.cub.2007.08.013.

Katz, P.S. (2011). Neural mechanisms underlying the evolvability of behaviour. Philosophical Transactions of the Royal Society B: Biological Sciences *366*, 2086–2099. https://doi.org/10.1098/RSTB.2010.0336.

Katz, P.S. (2016). Evolution of central pattern generators and rhythmic behaviours. Philosophical Transactions of the Royal Society B: Biological Sciences *371*. https://doi.org/10.1098/RSTB.2015.0057.

Kebschul, J.M., Richman, E.B., Ringach, N., Friedmann, D., Albarran, E., Kolluru, S.S., Jones, R.C., Allen, W.E., Wang, Y., Cho, S.W., et al. (2021). Cerebellar nuclei evolved by repeatedly duplicating a conserved cell-type set. Science (1979) *370*. https://doi.org/10.1126/science.abd5059.

Kernan, M., Cowan, D., and Zuker, C. (1994). Genetic dissection of mechanosensory transduction: Mechanoreception-defective mutations of drosophila. Neuron *12*, 1195–1206. https://doi.org/10.1016/0896-6273(94)90437-5.

Kim, C.K., Adhikari, A., and Deisseroth, K. (2017). Integration of optogenetics with complementary methodologies in systems neuroscience. Nature Reviews Neuroscience 2017 18:4 *18*, 222–235. https://doi.org/10.1038/nrn.2017.15.

Kirschner, M., and Gerhart, J. (1998). Evolvability. Proc Natl Acad Sci U S A *95*, 8420–8427. https://doi.org/10.1073/pnas.95.15.8420.

Kirszenblat, L., Pattabiraman, D., and Hilliard, M.A. (2011). LIN-44/Wnt Directs Dendrite Outgrowth through LIN-17/Frizzled in C. elegans Neurons. PLoS Biol *9*, e1001157. https://doi.org/10.1371/journal.pbio.1001157.

Kolodkin, A.L., and Tessier-Lavigne, M. (2011). Mechanisms and Molecules of Neuronal Wiring: A Primer. Cold Spring Harb Perspect Biol *3*, 1–14. https://doi.org/10.1101/CSHPERSPECT.A001727.

Kupfermann, I., and Weiss, K.R. (1978). The command neuron concept. Behavioral and Brain Sciences *1*, 3. https://doi.org/10.1017/S0140525X00059057.

Lacoste, J., Soula, H., Burg, A., Audibert, A., Darnat, P., Gho, M., and Louvet-Vallée, S. (2022). A neural progenitor mitotic wave is required for asynchronous axon outgrowth and morphology. Elife *11*. https://doi.org/10.7554/ELIFE.75746.

Landgraf, M., Sánchez-Soriano, N., Technau, G.M., Urban, J., and Prokop, A. (2003a). Charting the Drosophila neuropile: A strategy for the standardised characterisation of genetically amenable neurites. Dev Biol *260*, 207–225. https://doi.org/10.1016/S0012-1606(03)00215-X.

Landgraf, M., Jeffrey, V., Fujioka, M., Jaynes, J.B., and Bate, M. (2003b). Embryonic Origins of a Motor System: Motor Dendrites Form a Myotopic Map in Drosophila. PLoS Biol *1*, e41. https://doi.org/10.1371/journal.pbio.0000041.

Lei, Z., Henderson, K., and Keleman, K. (2022). A neural circuit linking learning and sleep in Drosophila long-term memory. Nature Communications 2022 13:1 *13*, 1–10. https://doi.org/10.1038/s41467-022-28256-1.

Leung, B., and Shimeld, S.M. (2019). Evolution of vertebrate spinal cord patterning. Developmental Dynamics *248*, 1028–1043. https://doi.org/10.1002/DVDY.77.

Levine, A.J., Lewallen, K.A., and Pfaff, S.L. (2012). Spatial organization of cortical and spinal neurons controlling motor behavior. Curr Opin Neurobiol *22*, 812–821. https://doi.org/10.1016/J.CONB.2012.07.002.

Levine, A.J., Hinckley, C.A., Hilde, K.L., Driscoll, S.P., Poon, T.H., Montgomery, J.M., and Pfaff, S.L. (2014). Identification of a cellular node for motor control pathways. Nat Neurosci *17*, 586–593. https://doi.org/10.1038/nn.3675.

Li, H.H., Kroll, J.R., Lennox, S.M., Ogundeyi, O., Jeter, J., Depasquale, G., and Truman, J.W. (2014). A GAL4 driver resource for developmental and behavioral studies on the larval CNS of Drosophila. Cell Rep *8*, 897–908. https://doi.org/10.1016/j.celrep.2014.06.065.

Lin, C.H., Senapati, B., Chen, W.J., Bansal, S., and Lin, S. (2022). Semaphorin 1a-mediated dendritic wiring of the Drosophila mushroom body extrinsic neurons. Proc Natl Acad Sci U S A *119*, e2111283119. https://doi.org/10.1073/PNAS.2111283119/SUPPL_FILE/PNAS.2111283119.SM01.AVI.

Luo, L., Callaway, E.M., and Svoboda, K. (2018). Genetic Dissection of Neural Circuits: A Decade of Progress. Neuron *98*, 256–281. https://doi.org/10.1016/J.NEURON.2018.03.040.

Lyuksyutova, A.I., Lu, C.-C., Milanesio, N., King, L.A., Guo, N., Wang, Y., Nathans, J., Tessier-Lavigne, M., and Zou, Y. (2003). Anterior-Posterior Guidance of Commissural Axons by Wnt-Frizzled Signaling. Science (1979) *302*, 1984–1988. https://doi.org/10.1126/science.1089610.

Manning, L., Heckscher, E.S., Purice, M.D., Roberts, J., Bennett, A.L., Kroll, J.R., Pollard, J.L., Strader, M.E., Lupton, J.R., Dyukareva, A. V, et al. (2012). A resource for manipulating gene expression and analyzing cis-regulatory modules in the Drosophila CNS. Cell Rep *2*, 1002–1013. https://doi.org/10.1016/j.celrep.2012.09.009.

Mark, B., Lai, S.L., Zarin, A.A., Manning, L., Pollington, H.Q., Litwin-Kumar, A., Cardona, A., Truman, J.W., and Doe, C.Q. (2021). A developmental framework linking neurogenesis and circuit formation in the drosophila cns. Elife *10*. https://doi.org/10.7554/ELIFE.67510.

Masson, J.B., Laurent, F., Cardona, A., Barre, C., Skatchkovsky, N., Zlatic, M., and Jovanic, T. (2020). Identifying neural substrates of competitive interactions and sequence transitions during mechanosensory responses in Drosophila. PLoS Genet *16*, e1008589. https://doi.org/10.1371/journal.pgen.1008589.

Miguel-Aliaga, I. (2004). Segment-specific prevention of pioneer neuron apoptosis by cell-autonomous, postmitotic Hox gene activity. Development *131*, 6093–6105. https://doi.org/10.1242/dev.01521.

Miguel-Aliaga, I., Thor, S., and Gould, A.P. (2008). Postmitotic specification of Drosophila insulinergic neurons from pioneer neurons. PLoS Biol *6*, 0538–0551. https://doi.org/10.1371/journal.pbio.0060058.

Nern, A., Pfeiffer, B.D., and Rubin, G.M. (2015). Optimized tools for multicolor stochastic labeling reveal diverse stereotyped cell arrangements in the fly visual system. Proceedings of the National Academy of Sciences *112*, E2967–E2976. https://doi.org/10.1073/pnas.1506763112.

Ohyama, T., Jovanic, T., Denisov, G., Dang, T.C., Hoffmann, D., Kerr, R.A., and Zlatic, M. (2013). High-Throughput Analysis of Stimulus-Evoked Behaviors in Drosophila Larva Reveals Multiple Modality-Specific Escape Strategies. PLoS One *8*, e71706. https://doi.org/10.1371/journal.pone.0071706.

Ohyama, T., Schneider-Mizell, C.M., Fetter, R.D., Aleman, J.V., Franconville, R., Rivera-Alba, M., Mensh, B.D., Branson, K.M., Simpson, J.H., Truman, J.W., et al. (2015). A multilevel multimodal circuit enhances action selection in Drosophila. Nature *520*, 633–639. https://doi.org/10.1038/nature14297.

Packard, M., Koo, E.S., Gorczyca, M., Sharpe, J., Cumberledge, S., and Budnik, V. (2002). The Drosophila Wnt, Wingless, Provides an Essential Signal for Pre- and Postsynaptic Differentiation. Cell *111*, 319–330. https://doi.org/10.1016/S0092-8674(02)01047-4.

Sakurai, A., Newcomb, J.M., Lillvis, J.L., and Katz, P.S. (2011). Different Roles for Homologous Interneurons in Species Exhibiting Similar Rhythmic Behaviors. Current Biology *21*, 1036–1043. https://doi.org/10.1016/j.cub.2011.04.040.

Salinas, P.C., and Zou, Y. (2008). Wnt Signaling in Neural Circuit Assembly. Http://Dx.Doi.Org/10.1146/Annurev.Neuro.31.060407.125649 *31*, 339–358. https://doi.org/10.1146/ANNUREV.NEURO.31.060407.125649.

Saltiel, P., Tresch, M.C., and Bizzi, E. (1998). Spinal Cord Modular Organization and Rhythm Generation: An NMDA Iontophoretic Study in the Frog. J Neurophysiol *80*, 2323–2339. https://doi.org/10.1152/jn.1998.80.5.2323.

Sato, M., Umetsu, D., Murakami, S., Yasugi, T., and Tabata, T. (2006). DWnt4 regulates the dorsoventral specificity of retinal projections in the Drosophila melanogaster visual system. Nat Neurosci *9*, 67–75. https://doi.org/10.1038/nn1604.

Seeholzer, L.F., Seppo, M., Stern, D.L., and Ruta, V. (2018). Evolution of a central neural circuit underlies Drosophila mate preferences. Nature 2018 559:7715 *559*, 564–569. https://doi.org/10.1038/s41586-018-0322-9.

Seroka, A.Q., and Doe, C.Q. (2019). The hunchback temporal transcription factor determines motor neuron axon and dendrite targeting in drosophila. Development (Cambridge) *146*. https://doi.org/10.1242/DEV.175570/VIDEO-2.

Shen, K., and Bargmann, C.I. (2003). The Immunoglobulin Superfamily Protein SYG-1 Determines the Location of Specific Synapses in C. elegans. Cell *112*, 619–630. https://doi.org/10.1016/S0092-8674(03)00113-2.

Sidak, Z. (1967). Rectangular Confidence Regions for the Means of Multivariate Normal Distributions. J Am Stat Assoc *62*, 626. https://doi.org/10.2307/2283989.

Takagi, S., Cocanougher, B.T., Niki, S., Miyamoto, D., Kohsaka, H., Kazama, H., Fetter, R.D., Truman, J.W., Zlatic, M., Cardona, A., et al. (2017). Divergent Connectivity of Homologous Command-like Neurons Mediates Segment-Specific Touch Responses in Drosophila. Neuron *96*, 1373-1387.e6. https://doi.org/10.1016/j.neuron.2017.10.030.

Tenedini, F.M., González, M.S., Hu, C., Pedersen, L.H., Petruzzi, M.M., Spitzweck, B., Wang, D., Richter, M., Petersen, M., Szpotowicz, E., et al. (2019). Maintenance of cell type-specific connectivity and circuit function requires Tao kinase. Nature Communications 2019 10:1 *10*, 1–16. https://doi.org/10.1038/s41467-019-11408-1.

Tessier-Lavigne, M., and Goodman, C.S. (1996). The Molecular Biology of Axon Guidance. Science (1979) *274*, 1123–1133. https://doi.org/10.1126/SCIENCE.274.5290.1123.

Tinbergen, N. (1951). The study of instinct (Oxford University Press).

Tosches, M.A. (2017). Developmental and genetic mechanisms of neural circuit evolution. Dev Biol *431*, 16–25. https://doi.org/10.1016/J.YDBIO.2017.06.016.

Tosches, M.A., Yamawaki, T.M., Naumann, R.K., Jacobi, A.A., Tushev, G., and Laurent, G. (2018). Evolution of pallium, hippocampus, and cortical cell types revealed by single-cell transcriptomics in reptiles. Science (1979) *360*, 881–888. https://doi.org/10.1126/SCIENCE.AAR4237.

Tresch, M.C., and Bizzi, E. (1999). Responses to spinal microstimulation in the chronically spinalized rat and their relationship to spinal systems activated by low threshold cutaneous stimulation. Exp Brain Res *129*, 401–416. .

Valdes-Aleman, J., Fetter, R.D., Sales, E.C., Heckman, E.L., Venkatasubramanian, L., Doe, C.Q., Landgraf, M., Cardona, A., and Zlatic, M. (2021). Comparative Connectomics Reveals How Partner Identity, Location, and Activity Specify Synaptic Connectivity in Drosophila. Neuron *109*, 105-122.e7. https://doi.org/10.1016/J.NEURON.2020.10.004.

Wiersma, C.A.G., and Ikeda, K. (1964). Interneurons commanding swimmeret movements in the crayfish, Procambarus clarki (girard). Comp Biochem Physiol *12*, 509–525. https://doi.org/10.1016/0010-406X(64)90153-7.

Wu, C., and Nusse, R. (2002). Ligand receptor interactions in the Wnt signaling pathway in Drosophila. J Biol Chem *277*, 41762–41769. https://doi.org/10.1074/jbc.M207850200.

Wu, F., Deng, B., Xiao, N., Wang, T., Li, Y., Wang, R., Shi, K., Luo, D.G., Rao, Y., and Zhou, C. (2020). A neuropeptide regulates fighting behavior in drosophila melanogaster. Elife *9*. https://doi.org/10.7554/ELIFE.54229.

Xie, X., Tabuchi, M., Corver, A., Duan, G., Wu, M.N., and Kolodkin, A.L. (2019). Semaphorin 2b Regulates Sleep-Circuit Formation in the Drosophila Central Brain. Neuron *104*, 322-337.e14. https://doi.org/10.1016/J.NEURON.2019.07.019.

Xu, C., Theisen, E., Maloney, R., Peng, J., Santiago, I., Yapp, C., Werkhoven, Z., Rumbaut, E., Shum, B., Tarnogorska, D., et al. (2019). Control of Synaptic Specificity by Establishing a Relative Preference for Synaptic Partners. Neuron *103*, 865-877.e7. https://doi.org/10.1016/J.NEURON.2019.06.006.

Yoshikawa, S., McKinnon, R.D., Kokel, M., and Thomas, J.B. (2003). Wnt-mediated axon guidance via the Drosophila Derailed receptor. Nature *422*, 583–588.

https://doi.org/10.1038/nature01522.

Figure 1

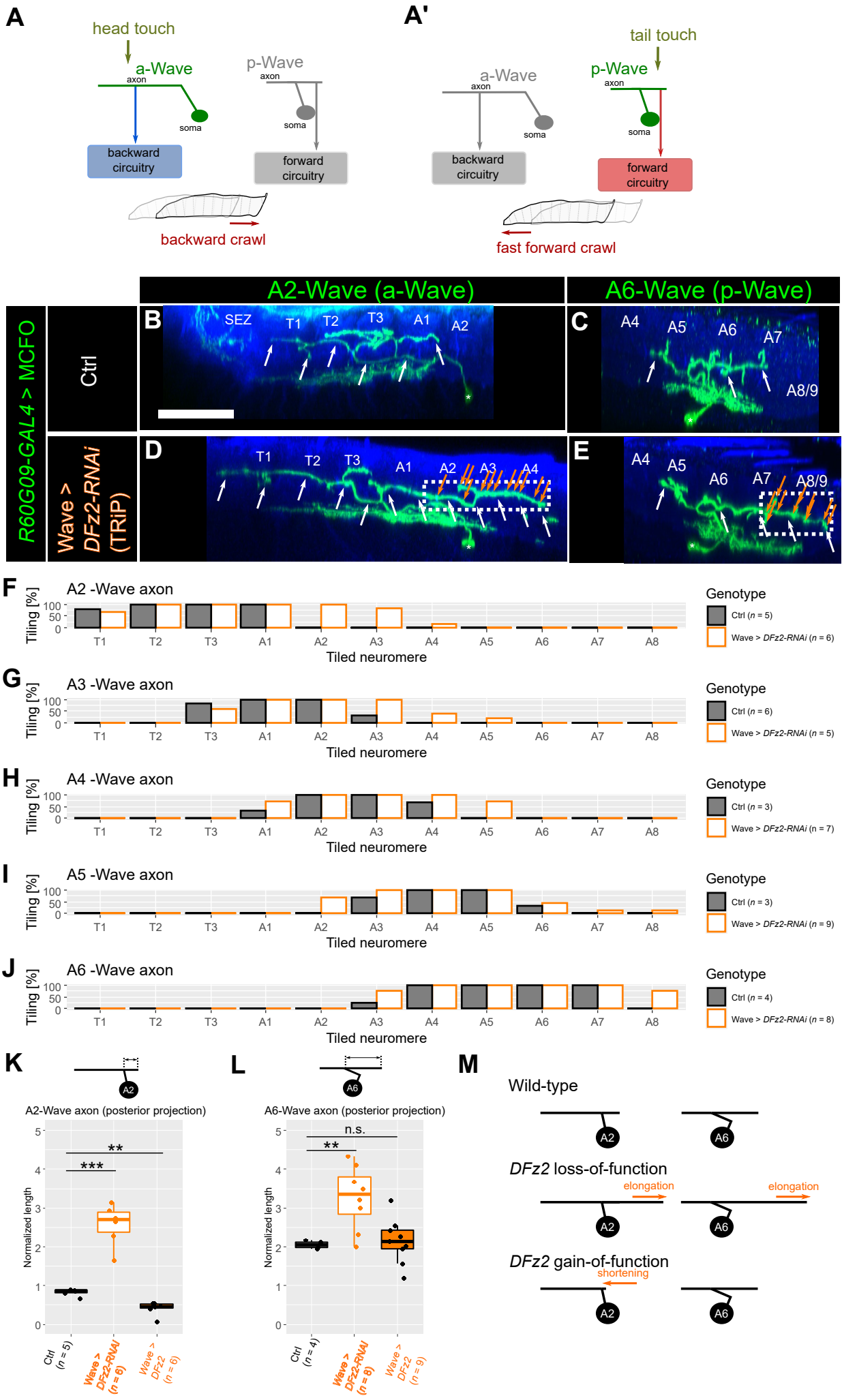
A
head touch
a-Wave
axon
soma
backward circuitry
p-Wave
axon
soma
forward circuitry
backward crawl
A'
a-Wave
axon
soma
backward circuitry
tail touch
p-Wave
axon
soma
forward circuitry
fast forward crawl
A2-Wave (a-Wave)
A6-Wave (p-Wave)
R60G09-GAL4 > MCFO
Ctrl
Wave > DFz2-RNAi (TRiP)
B
SEZ
T1
T2
T3
A1
A2
C
A4
A5
A6
A7
A8/9
D
T1
T2
T3
A1
A2
A3
A4
E
A4
A5
A6
A7
A8/9
F
A2 -Wave axon
Tiling [%]
Tiled neuromere
Genotype
Ctrl (n = 5)
Wave > DFz2-RNAi (n = 6)
G
A3 -Wave axon
Ctrl (n = 6)
Wave > DFz2-RNAi (n = 5)
H
A4 -Wave axon
Ctrl (n = 3)
Wave > DFz2-RNAi (n = 7)
I
A5 -Wave axon
Ctrl (n = 3)
Wave > DFz2-RNAi (n = 9)
J
A6 -Wave axon
Ctrl (n = 4)
Wave > DFz2-RNAi (n = 8)
K
A2-Wave axon (posterior projection)
Normalized length
**
***
Ctrl (n = 5)
Wave > DFz2-RNAi (n = 6)
Wave > DFz2 (n = 6)
L
A6-Wave axon (posterior projection)
n.s.
**
Ctrl (n = 4)
Wave > DFz2-RNAi (n = 8)
Wave > DFz2 (n = 9)
M
Wild-type
DFz2 loss-of-function
elongation
DFz2 gain-of-function
shortening

Figure 2

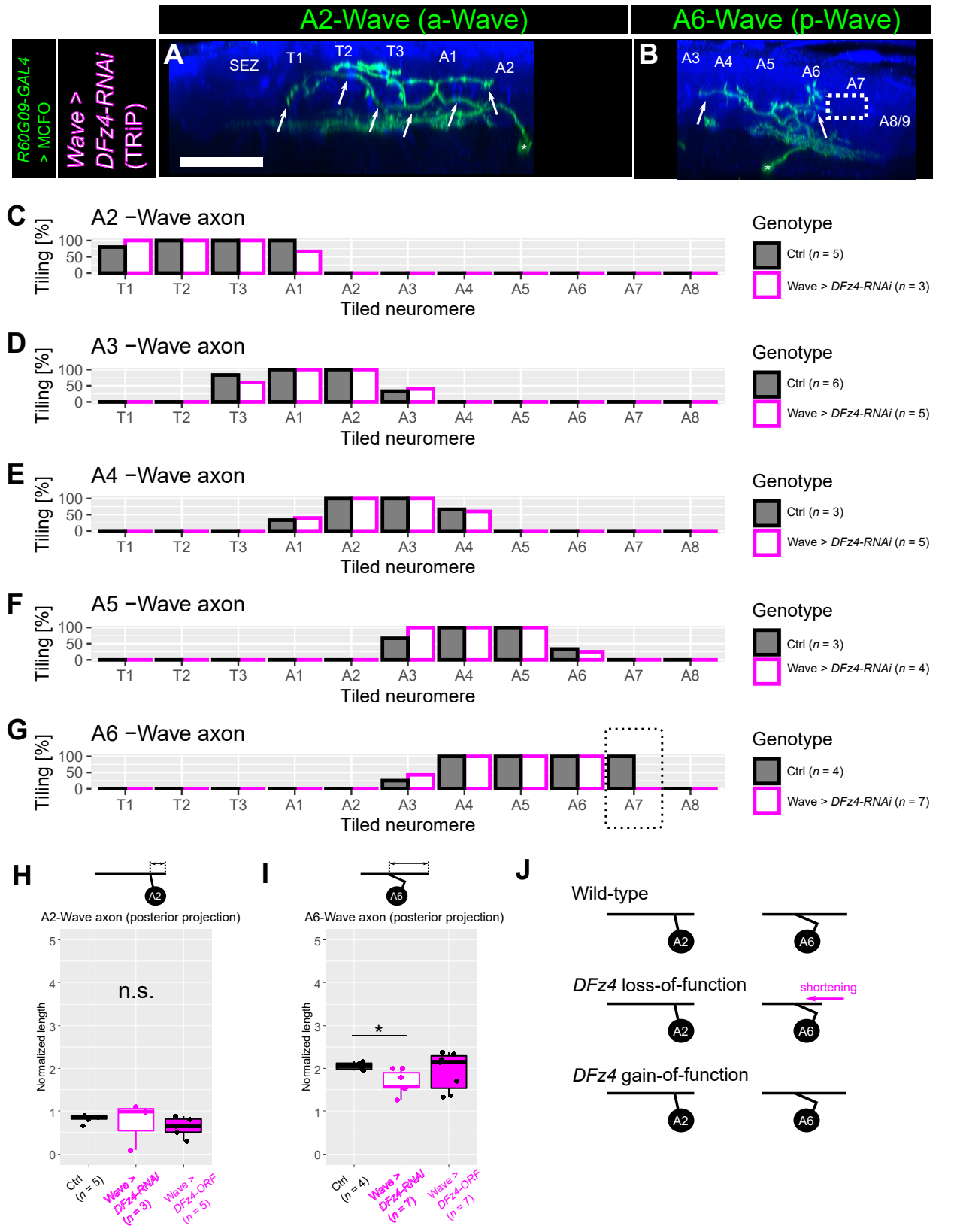
A2-Wave (a-Wave)
A6-Wave (p-Wave)
R60G09-GAL4 > MCFO
Wave > DFz4-RNAi (TRiP)
A
SEZ
T1
T2
T3
A1
A2
B
A3
A4
A5
A6
A7
A8/9
C
A2 −Wave axon
D
A3 −Wave axon
E
A4 −Wave axon
F
A5 −Wave axon
G
A6 −Wave axon
Tiling [%]
Tiled neuromere
Genotype
Ctrl (n = 5)
Wave > DFz4-RNAi (n = 3)
Ctrl (n = 6)
Wave > DFz4-RNAi (n = 5)
Ctrl (n = 3)
Wave > DFz4-RNAi (n = 5)
Ctrl (n = 3)
Wave > DFz4-RNAi (n = 4)
Ctrl (n = 4)
Wave > DFz4-RNAi (n = 7)
H
A2-Wave axon (posterior projection)
n.s.
Normalized length
Ctrl (n = 5)
Wave > DFz4-RNAi (n = 3)
Wave > DFz4-ORF (n = 5)
I
A6-Wave axon (posterior projection)
*
Ctrl (n = 4)
Wave > DFz4-RNAi (n = 7)
Wave > DFz4-ORF (n = 7)
J
Wild-type
DFz4 loss-of-function
shortening
DFz4 gain-of-function
A2
A6

Figure 3

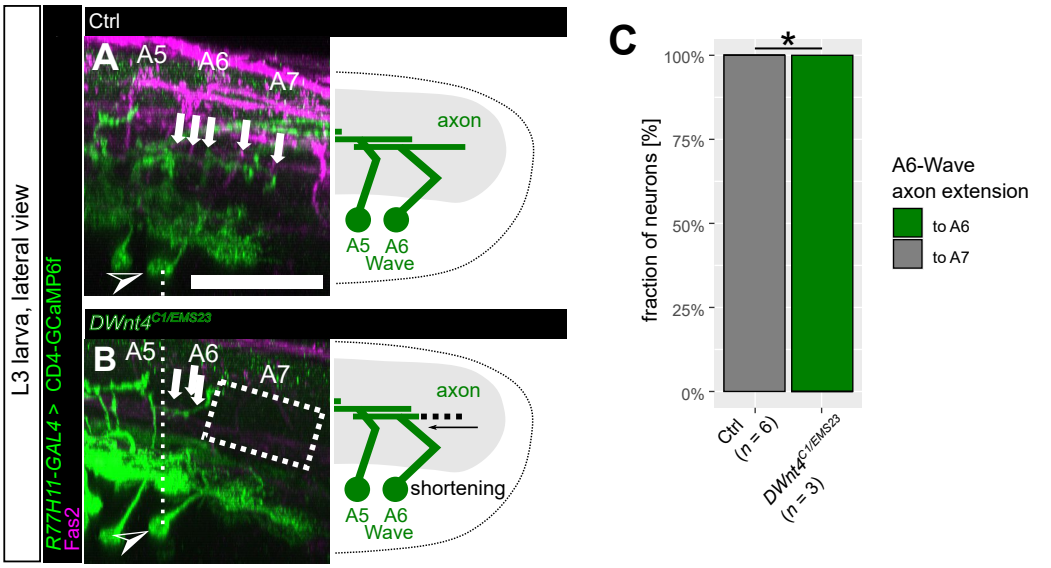
L3 larva, lateral view
R77H11-GAL4 > CD4-GCaMP6f
Fas2
Ctrl
A
A5
A6
A7
axon
A5 A6
Wave
DWnt4C1/EMS23
B
A5
A6
A7
axon
shortening
A5 A6
Wave
C
100%
75%
50%
25%
0%
fraction of neurons [%]
*
Ctrl
(n = 6)
DWnt4C1/EMS23
(n = 3)
A6-Wave
axon extension
to A6
to A7

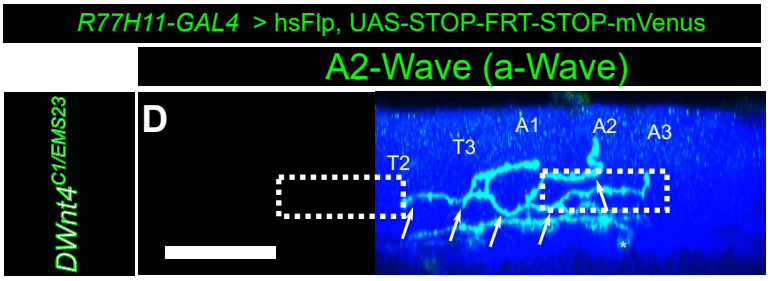
R77H11-GAL4 > hsFlp, UAS-STOP-FRT-STOP-mVenus
A2-Wave (a-Wave)
DWnt4C1/EMS23
D
T2
T3
A1
A2
A3

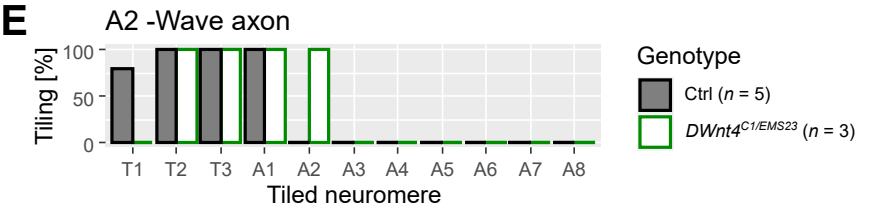
E
A2 -Wave axon
Tiling [%]
100
50
0
T1
T2
T3
A1
A2
A3
A4
A5
A6
A7
A8
Tiled neuromere
Genotype
Ctrl (n = 5)
DWnt4C1/EMS23 (n = 3)

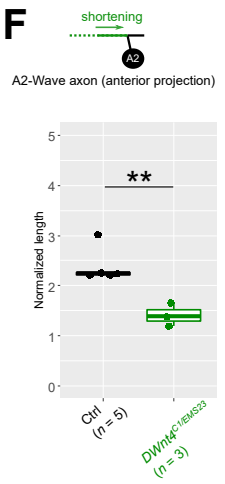
F
shortening
A2
A2-Wave axon (anterior projection)
Normalized length
**
Ctrl
(n = 5)
DWnt4C1/EMS23
(n = 3)

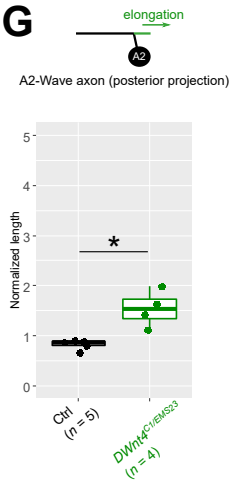
G
elongation
A2
A2-Wave axon (posterior projection)
Normalized length
*
Ctrl
(n = 5)
DWnt4C1/EMS23
(n = 4)

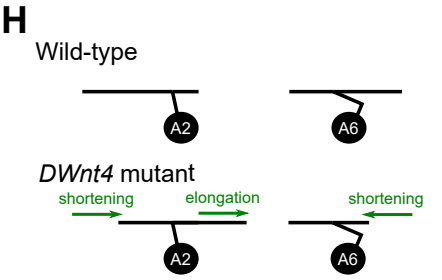
H
Wild-type
A2
A6
DWnt4 mutant
shortening
elongation
A2
shortening
A6

Figure 4

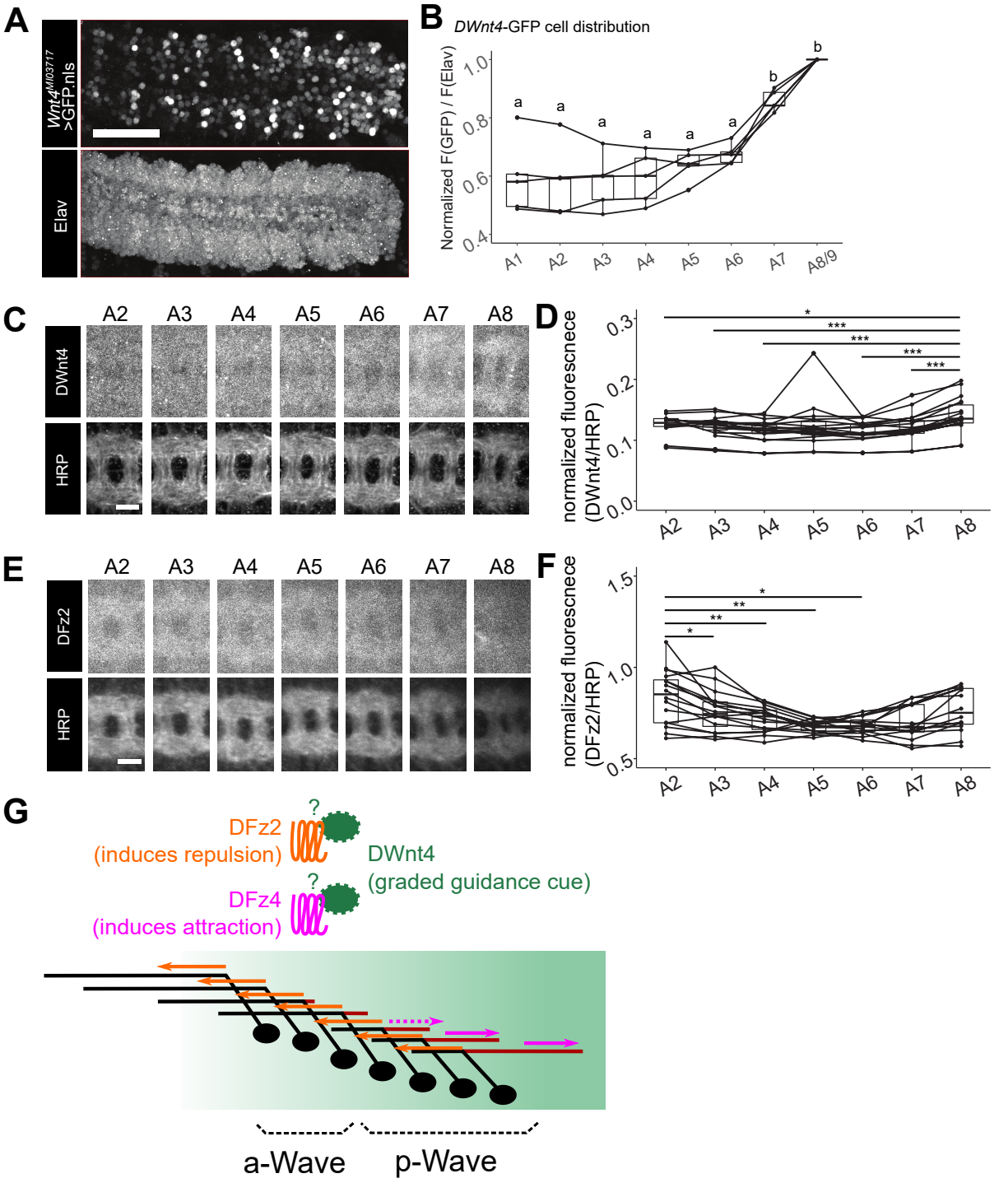
A
Wnt4MI03717 >GFP.nls
Elav
B
DWnt4-GFP cell distribution
Normalized F(GFP) / F(Elav)
1.0
0.8
0.6
0.4
a
a
a
a
a
a
b
b
b
A1
A2
A3
A4
A5
A6
A7
A8/9
C
A2
A3
A4
A5
A6
A7
A8
DWnt4
HRP
D
normalized fluorescnece (DWnt4/HRP)
0.3
0.2
0.1
0.0
*
***
***
***
***
A2
A3
A4
A5
A6
A7
A8
E
A2
A3
A4
A5
A6
A7
A8
DFz2
HRP
F
normalized fluorescnece (DFz2/HRP)
1.5
1.0
0.5
*
**
**
*
A2
A3
A4
A5
A6
A7
A8
G
DFz2
(induces repulsion)
?
DWnt4
(graded guidance cue)
DFz4
(induces attraction)
?
a-Wave
p-Wave

Figure 5

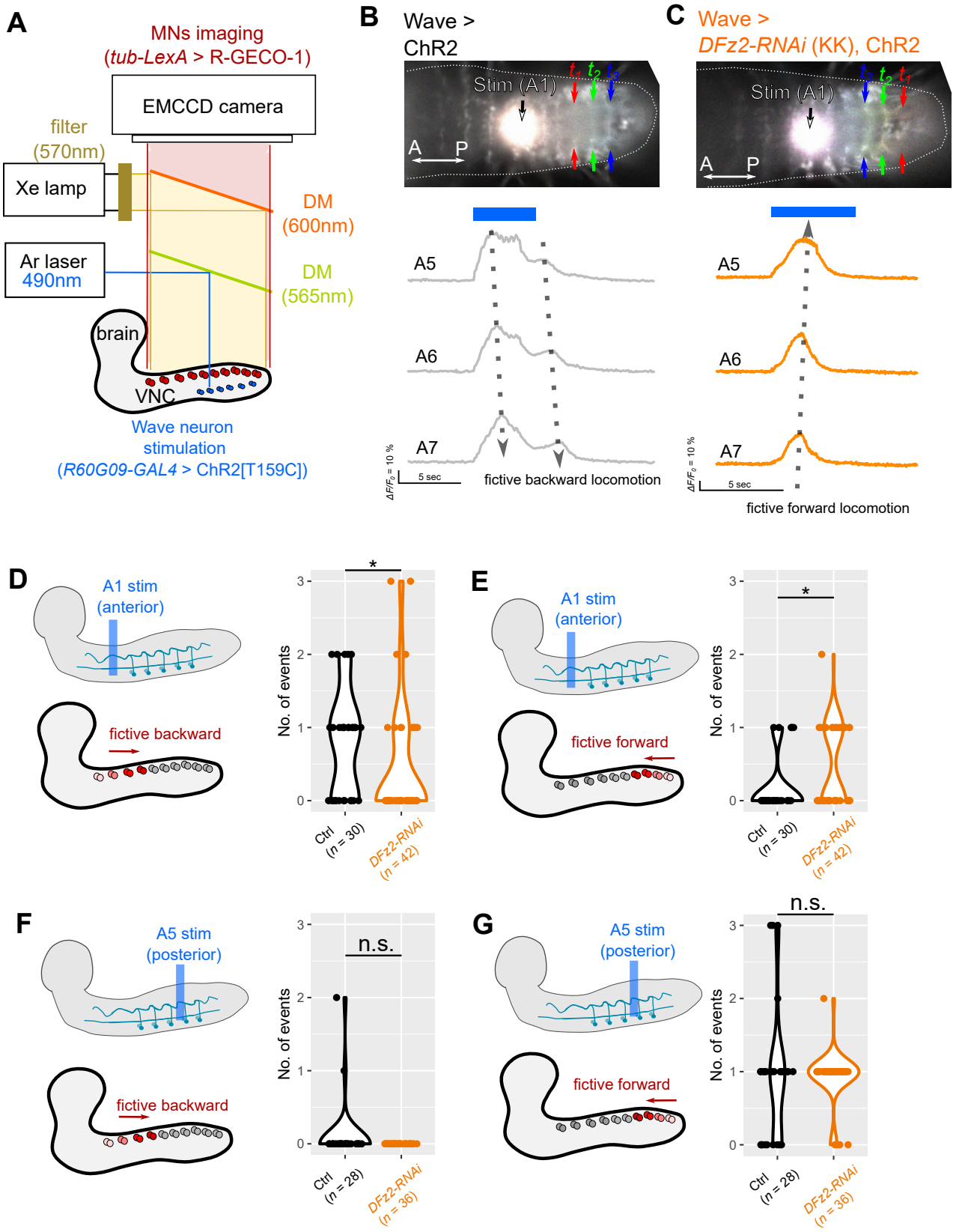
A
MNs imaging
(tub-LexA > R-GECO-1)
EMCCD camera
filter
(570nm)
Xe lamp
DM
(600nm)
Ar laser
490nm
DM
(565nm)
brain
VNC
Wave neuron
stimulation
(R60G09-GAL4 > ChR2[T159C])
B
Wave >
ChR2
Stim (A1)
A
P
A5
A6
A7
5 sec
fictive backward locomotion
C
Wave >
DFz2-RNAi (KK), ChR2
Stim (A1)
A
P
A5
A6
A7
5 sec
fictive forward locomotion
D
A1 stim
(anterior)
fictive backward
No. of events
Ctrl
(n = 30)
DFz2-RNAi
(n = 42)
E
A1 stim
(anterior)
fictive forward
No. of events
Ctrl
(n = 30)
DFz2-RNAi
(n = 42)
F
A5 stim
(posterior)
fictive backward
n.s.
No. of events
Ctrl
(n = 28)
DFz2-RNAi
(n = 36)
G
A5 stim
(posterior)
fictive forward
n.s.
No. of events
Ctrl
(n = 28)
DFz2-RNAi
(n = 36)

Figure 6

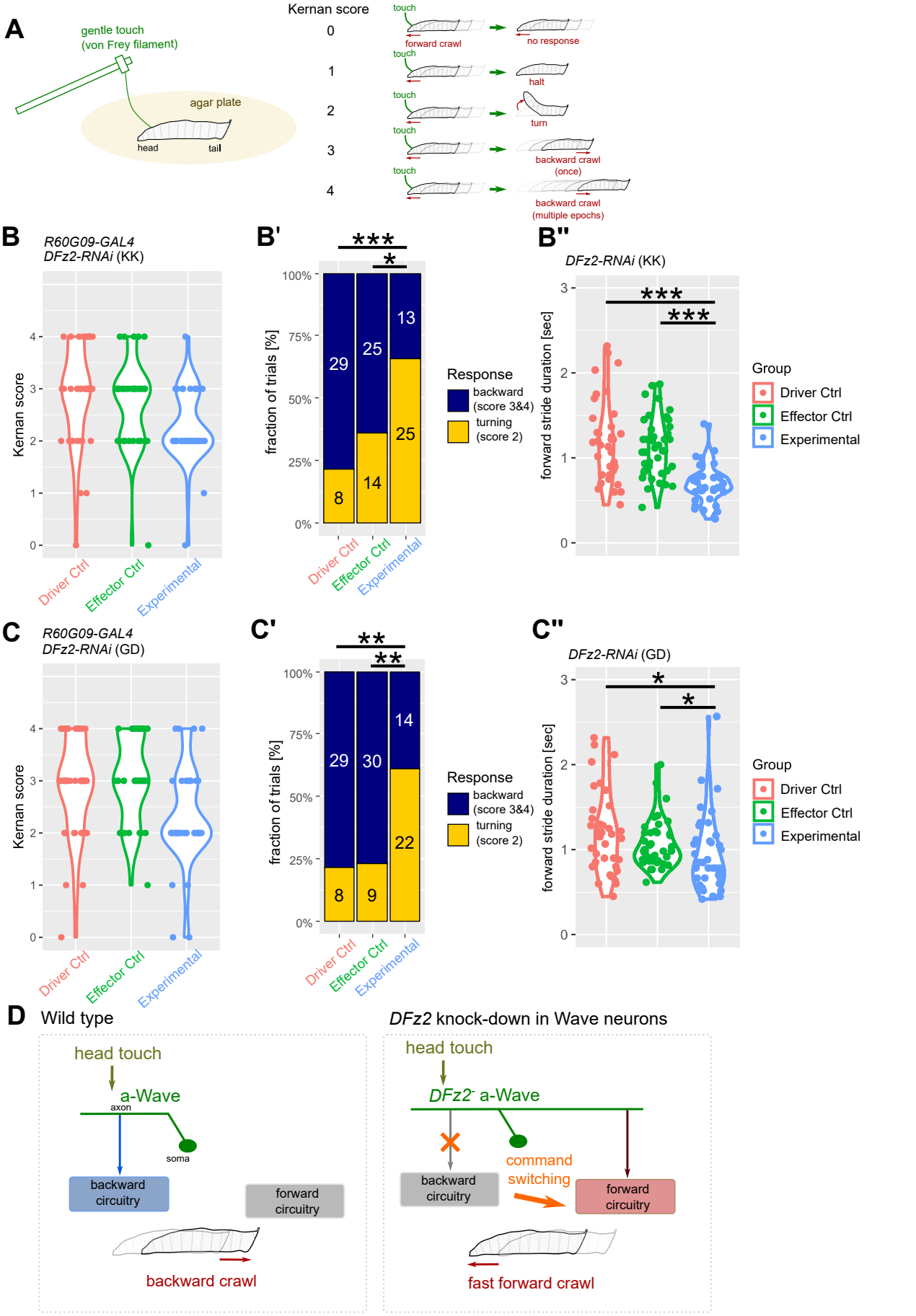
A
gentle touch
(von Frey filament)
agar plate
head
tail
Kernan score
0
1
2
3
4
touch
forward crawl
no response
halt
turn
backward crawl
(once)
backward crawl
(multiple epochs)
B
R60G09-GAL4
DFz2-RNAi (KK)
Kernan score
Driver Ctrl
Effector Ctrl
Experimental
B'
***
*
fraction of trials [%]
100%
75%
50%
25%
0%
29
8
25
14
13
25
Response
backward
(score 3&4)
turning
(score 2)
B''
DFz2-RNAi (KK)
forward stride duration [sec]
***
***
Group
Driver Ctrl
Effector Ctrl
Experimental
C
R60G09-GAL4
DFz2-RNAi (GD)
C'
**
**
29
8
30
9
14
22
C''
DFz2-RNAi (GD)
*
*
D
Wild type
head touch
a-Wave
axon
soma
backward
circuitry
forward
circuitry
backward crawl
DFz2 knock-down in Wave neurons
DFz2- a-Wave
command
switching
fast forward crawl